IN-24
88791
P.31

NASA
Technical
Paper
3195

May 1992

Buckling Behavior of Long Symmetrically Laminated Plates Subjected to Combined Loadings

Michael P. Nemeth

(NASA-TP-3195) BUCKLING BEHAVIOR OF LONG SYMMETRICALLY LAMINATED PLATES SUBJECTED TO COMBINED LOADINGS (NASA) 31 p CSCL 11D

N92-25160

Unclas
H1/24 0088791

NASA

NASA
Technical
Paper
3195

1992

Buckling Behavior of Long Symmetrically Laminated Plates Subjected to Combined Loadings

Michael P. Nemeth
Langley Research Center
Hampton, Virginia

National Aeronautics and
Space Administration

Office of Management

Scientific and Technical
Information Program

The use of trademarks or names of manufacturers in this report is for accurate reporting and does not constitute an official endorsement, either expressed or implied, of such products or manufacturers by the National Aeronautics and Space Administration.

Abstract

A parametric study is presented of the buckling behavior of infinitely long, symmetrically laminated anisotropic plates subjected to combined loadings. The loading conditions considered are axial tension and compression, transverse tension and compression, and shear. Results obtained using a special-purpose analysis, well-suited for parametric studies, are presented for clamped and simply supported plates. Moreover, results are presented for some common laminate constructions, and generic buckling design charts are presented for a wide range of parameters. The generic design charts are presented in terms of useful nondimensional parameters, and the dependence of the nondimensional parameters on laminate fiber orientation, stacking sequence, and material properties is discussed.

An important finding of the study is that the effects of anisotropy are much more pronounced in shear-loaded plates than in compression-loaded plates. In addition, the effects of anisotropy on plates subjected to combined loadings are generally manifested as a phase shift of self-similar buckling interaction curves. A practical application of this phase shift is that the buckling resistance of long plates can be improved by applying a shear loading with a specific orientation. In all cases considered in the study, the buckling coefficients of infinitely long plates are found to be independent of the bending stiffness ratio $(D_{11}/D_{22})^{1/4}$.

Introduction

Buckling behavior of laminated plates is a topic of fundamental importance in the design of aerospace vehicle structures. Often the sizing of many subcomponents of these vehicles is determined by stability constraints in addition to other constraints such as stiffness and strength. One typical subcomponent of great practical importance in structural design is the long rectangular plate. These plates routinely appear as subcomponents of stiffened panels used for wings, ribs, and spars. In addition, long plates commonly appear as subcomponents of semimonocoque shells used for fuselage structure, liquid-propellant booster tankage, and booster interstage structure. Buckling results for infinitely long plates are important because they provide a lower bound on the behavior of finite-length rectangular plates, and they provide information that is useful in explaining the behavior of finite-length plates.

Understanding the buckling behavior of symmetrically laminated plates is an important part of the search for ways to exploit plate orthotropy and anisotropy to reduce structural weight of aircraft and launch vehicles. Symmetrically laminated plates can exhibit anisotropy in the form of material-induced coupling between pure bending and twisting deformations. This coupling generally yields buckling modes that are skewed in appearance, as depicted in figure 1. The effects of anisotropy on the buckling behavior of these compression-loaded plates is well-known (e.g., refs. 1 and 2). However, the effects of anisotropy on symmetrically laminated plates subjected to shear loadings and various other combined loadings are generally not as well-understood.

Symmetrically laminated plates can have many different constructions because of the wide variety of material systems, fiber orientations, and stacking sequences that can be used to construct a laminate. Thus, it is extremely useful for the designer to have a means of assessing the performance of various laminated plates on a common and unbiased basis. The use of nondimensional parameters can provide this means for assessing laminate performance. Moreover, the use of nondimensional parameters permits buckling results to be presented in a concise manner on one or more plots as a series of generic curves that span the complete range of plate dimensions, loading combinations, boundary conditions, laminate construction, and material properties. An added benefit is that the generic curves also furnish the designer with an overall indication of the sensitivity of the structural response to changes in the design parameters. Examples of generic design charts that use nondimensional parameters are presented in references 3 and 4 for buckling and postbuckling of orthotropic plates.

The major objectives of the present paper are to indicate the effects of plate bending orthotropy and anisotropy on the buckling of plates subjected to combined loads, and to present generic design charts that indicate the buckling behavior of long plates for a wide range of parameters in a concise manner. The loading conditions considered in this paper are axial tension and compression, transverse tension and compression, and shear loadings. Results are presented herein for plates with the two opposite long edges clamped or simply supported. A substantial number of generic buckling curves that are applicable to a wide range of laminate constructions are presented in the present paper.

Symbols

A_n, B_n	displacement amplitudes (see eq. (8)), in.
b	plate width (see fig. 1), in.
D_{11}, D_{12}, D_{22}, D_{66}	orthotropic plate bending stiffnesses, in-lb
D_{16}, D_{26}	anisotropic plate bending stiffnesses, in-lb
E_1, E_2, G_{12}	lamina moduli, psi
K_x, K_y, K_s	nondimensional buckling coefficients associated with axial compression, transverse compression, and shear loadings (see eqs. (5), (6), and (7), respectively)
m	laminate stacking-sequence number
N_x, N_y, N_{xy}	membrane prebuckling stress resultants (see fig. 1), lb/in.
N_x^{cr}, N_y^{cr}, N_{xy}^{cr}	values of membrane stress resultants at buckling, lb/in.
$\bar{p}$, $\bar{p}_{cr}$	nondimensional loading parameter and corresponding value at buckling, respectively
w_N	out-of-plane displacement field at buckling (see eq. (8)), in.
x, y	plate coordinate system (see fig. 1), in.
α, β, γ, δ	nondimensional parameters defined by equations (1), (2), (3), and (4), respectively
$\eta = y/b$, $\xi = x/\lambda$	nondimensional plate coordinates
θ	fiber orientation angle (see fig. 1), deg
λ	half-wavelength of buckling mode (see fig. 1), in.
ν_{12}	lamina major Poisson's ratio
Φ_n, Ψ_n	kinematically admissible basis functions (see eq. (8))

Approach

The objectives of the present study are achieved herein in two different ways. In the first way, the effects of plate orthotropy and anisotropy are presented in an implicit manner for symmetrically laminated angle-ply plates. This family of laminates is denoted herein by the symbols $[(\pm\theta)_m]_s$, where θ is the fiber orientation angle shown in figure 1 (given in units of degrees) and m is the stacking-sequence number that indicates the number of times that the plies in parentheses are repeated. This family of laminates was chosen because varying the laminate parameters θ and m encompasses a wide range of plate bending orthotropy and bending anisotropy. The term *implicit* is used above to reflect the fact that for the angle-ply laminates, as well as for all other laminates, the plate orthotropy and anisotropy are implicit functions of laminate fiber orientation and stacking sequence and do not typically vary independently. This implicit way of assessing plate behavior is generally the approach that is the most familiar to aerospace vehicle designers.

A second way to characterize the effects of plate orthotropy and anisotropy uses the nondimensional parameters presented in reference 1. These nondimensional parameters are used in the present paper to show the effects of plate orthotropy and anisotropy on buckling behavior in a somewhat more explicit manner. For example, buckling results are presented in the present paper as a function of two parameters that characterize plate orthotropy and two parameters that characterize plate anisotropy. By varying each parameter in a systematic manner, the effects of orthotropy and anisotropy on buckling can be assessed independently. An important step in this assessment is to establish an understanding of how laminate fiber orientation, stacking sequence, and material properties affect the values of the nondimensional

parameters. Thus, results are also presented herein that indicate the effects of laminate construction on the nondimensional parameters for a few selected laminates. Material properties considered herein are representative of high-strength graphite-epoxy material, ultrahigh-modulus graphite-epoxy material, S-glass[1]-epoxy material, Kevlar[2]-epoxy material, boron-epoxy material, and boron-aluminum material.

Analysis Description

Often in preparing generic design charts for buckling of a single plate element, a special-purpose analysis is preferred over a general-purpose analysis code, such as a finite element code, because of the cost and effort involved in generating a large number of results with a general-purpose analysis code. The results presented in the present paper have been obtained using such a special-purpose analysis. A brief description of the analysis is presented subsequently.

The buckling analysis used in the present study is based on the classical Rayleigh-Ritz variational method and is derived explicitly in terms of the nondimensional parameters defined in reference 1. Deriving the analysis in this manner inherently makes the resulting computer code well-suited for parametric studies. The nondimensional parameters used are given by

$$\alpha = \frac{b}{\lambda}\left(\frac{D_{11}}{D_{22}}\right)^{1/4} \tag{1}$$

$$\beta = \frac{D_{12} + 2D_{66}}{\sqrt{D_{11}D_{22}}} \tag{2}$$

$$\gamma = \frac{D_{16}}{\left(D_{11}^3 D_{22}\right)^{1/4}} \tag{3}$$

$$\delta = \frac{D_{26}}{\left(D_{11}D_{22}^3\right)^{1/4}} \tag{4}$$

where λ is the half-wavelength of the buckling mode and b is the plate width shown in figure 1. The subscripted D terms appearing in the equations are the plate bending stiffnesses of classical laminated plate theory. The parameters α and β characterize plate bending orthotropy, and the parameters γ and δ characterize plate bending anisotropy. The parameters defined by equations (2) through (4) depend only on the plate bending stiffnesses, whereas the parameter α depends on the buckle aspect ratio λ/b also. Without loss of generality, and as a matter of convenience, the nondimensional parameter $(D_{11}/D_{22})^{1/4}$ is used in the present study in the place of the parameter α to assess plate bending orthotropy.

In addition to $(D_{11}/D_{22})^{1/4}$, β, γ, and δ, three additional nondimensional quantities are used to characterize buckling resistance, and they are given by

$$K_x = \frac{N_x^{cr} b^2}{\pi^2 \sqrt{D_{11}D_{22}}} \tag{5}$$

$$K_y = \frac{N_y^{cr} b^2}{\pi^2 D_{22}} \tag{6}$$

$$K_s = \frac{N_{xy}^{cr} b^2}{\pi^2 \left(D_{11}D_{22}^3\right)^{1/4}} \tag{7}$$

The quantities K_x, K_y, and K_s are referred to herein as the axial compression buckling coefficient, the transverse compression buckling coefficient, and the shear buckling coefficient, respectively. Each of the loading conditions associated with these buckling coefficients is shown in figure 1. The positive-valued compressive stress resultants and the shear stress resultant corresponding to the loadings are denoted by N_x, N_y, and N_{xy}, respectively. The stress resultants appearing in the buckling coefficients correspond to critical values associated with the onset of buckling.

In the buckling analysis, the infinitely long plates are assumed to have uniform thickness and material properties that do not vary along the plate length and width. In addition, the uniform biaxial and shear loadings and the boundary conditions do not vary along the plate length. Under these conditions, infinitely long plates have periodic buckling modes that exhibit either inversion symmetry or inversion antisymmetry with respect to a given reference point. The buckling mode depicted in figure 1 corresponds to either inversion symmetry or antisymmetry depending on the selection of the reference point. The presence of the periodicity and inversion symmetry or antisymmetry in the plate buckling mode aids in simplifying the buckling analysis.

An important characteristic of an infinitely long plate that possesses a periodic buckling mode is that a basic repetitive buckle pattern can be identified from which the overall buckling mode can be constructed by axial translation of the pattern. The selection of the basic repetitive buckle pattern is not unique, and thus one may choose it to simplify the buckling analysis further. In the present study, the basic repetitive buckle pattern was chosen because it possesses inversion symmetry about its geometric

[1]S-glass: Trademark of the Ferro Corporation.
[2]Kevlar: Trademark of E. I. duPont de Nemours & Co., Inc.

center. This simplification is important in that it permits the elimination of superfluous terms in the kinematically admissible series used to describe the buckling mode, which in turn simplifies the ensuing analysis and reduces the number of computations required to obtain an accurate result. The mathematical expression used in the variational analysis to describe the buckle pattern is given by

$$w_N(\xi,\eta) = \sin\ \pi\xi \sum_{n=1}^{N} A_n\ \Phi_n(\eta) + \cos\ \pi\xi \sum_{n=1}^{N} B_n\ \Psi_n(\eta) \quad (8)$$

where $\xi = x/\lambda$ and $\eta = y/b$ are nondimensional coordinates (see fig. 1), w_N is the out-of-plane displacement field, and A_n and B_n are the unknown displacement amplitudes. In accordance with the Raleigh-Ritz method, the basis functions $\Phi_n(\eta)$ and $\Psi_n(\eta)$ are required to satisfy the kinematic boundary conditions on the plate edges at $\eta = 0$ and 1. For the simply supported plates, the basis functions used in the analysis are given by

$$\Phi_n(\eta) = \sin 2n\pi\eta \quad (9a)$$

$$\Psi_n(\eta) = \sin(2n-1)\pi\eta \quad (9b)$$

for values of $n = 1, 2, 3, \ldots, N$. Similarly, for the clamped plates, the basis functions are given by

$$\Phi_n(\eta) = \cos(2n-1)\pi\eta - \cos(2n+1)\pi\eta \quad (10a)$$

$$\Psi_n(\eta) = \cos 2(n-1)\pi\eta - \cos 2n\pi\eta \quad (10b)$$

Algebraic equations governing buckling of long plates are obtained by substituting the series expansion for the buckling mode given by equation (8) into the second variation of the total potential energy and then computing the integrals appearing in the second variation in closed form. The resulting equations constitute a generalized eigenvalue problem that depends on the aspect ratio of the buckle pattern λ/b (see fig. 1) and the nondimensional parameters defined by equations (1) through (4). The inplane loadings are expressed in terms of a loading parameter $\tilde{p}$ that is increased monotonically until buckling occurs. The smallest eigenvalue of the problem $\tilde{p}_{cr}$ corresponds to buckling and is found by specifying a value of λ/b and solving the corresponding generalized eigenvalue problem for its smallest eigenvalue. This process is repeated for successive values of λ/b until the absolute smallest eigenvalue is found. The absolute smallest eigenvalue corresponds to $\tilde{p}_{cr}$.

Results obtained using the analysis described in the present paper were compared with results for isotropic and specially orthotropic plates published in the technical literature for several loading cases and boundary conditions. (See refs. 4 through 10.) Results for anisotropic plates were also compared with results obtained using the computer code VIPASA. (See ref. 11.) In all comparisons, results obtained from the analysis used in the present study were found to be within a few percent of the results published in references 4 through 10 and the VIPASA results.

Laminate Construction and Nondimensional Parameters

To characterize plate buckling behavior in terms of nondimensional parameters, it is important to understand how laminate fiber orientation, stacking sequence, and material properties affect their values. To accomplish this task and to determine the numerical range of the nondimensional parameters for typical balanced symmetric laminates, results are presented in this section for $[(\pm\theta)_m]_s$ angle-ply laminates, $[(\pm45/0/90)_m]_s$ and $[(0/90/\pm45)_m]_s$ quasi-isotropic laminates, and $[(\pm45/0_2)_m]_s$ and $[(\pm45/90_2)_m]_s$ laminates typically referred to as *orthotropic laminates*. Each of these laminates possesses specially orthotropic membrane deformation states prior to buckling. (That is, the A_{16} and A_{26} laminate constitutive terms are zero-valued.)

Effects of Fiber Orientation and Stacking Sequence

Values of the nondimensional parameters β, γ, δ, and the parameter $(D_{11}/D_{22})^{1/4}$ are shown in figures 2 and 3 for $[\pm\theta]_s$ and $[(\pm45)_m]_s$ angle-ply laminates, respectively. Similar results are presented in figure 4 for $[(\pm45/0/90)_m]_s$ and $[(0/90/\pm45)_m]_s$ quasi-isotropic laminates, and in figure 5 for $[(\pm45/0_2)_m]_s$ and $[(\pm45/90_2)_m]_s$ laminates. All results presented in these figures are for laminates with plies made of a typical graphite-epoxy material having a longitudinal modulus E_1 of 18.5×10^6 psi, a transverse modulus E_2 of 1.6×10^6 psi, an inplane shear modulus G_{12} of 0.832×10^6 psi, a major Poisson's ratio ν_{12} of 0.35, and a nominal ply thickness of 0.005 in.

For the angle-ply laminates, the anisotropic parameters γ and δ have maximum values at $\theta = 39°$ and 51°, respectively (see fig. 2), and their values diminish monotonically as the number of plies increases (see fig. 3). Between the values of 39° and 51°, values of γ (and similarly δ) vary by only a couple of percent. The orthotropic parameters β and $(D_{11}/D_{22})^{1/4}$ have maximum values at $\theta = 45°$

and 0°, respectively, and their values remain constant as the number of plies increases.

For the 0/45/90 family of quasi-isotropic laminates, the anisotropic parameters γ and δ shown in figure 4 asymptotically approach zero from above as the number of plies increases. The solid curves and dashed curves shown in figure 4 indicate results for the $[(0/90/\pm45)_m]_s$ and $[(\pm45/0/90)_m]_s$ laminates, respectively. The results in figure 4 indicate that the orthotropic parameters β and $(D_{11}/D_{22})^{1/4}$ for the $[(\pm45/0/90)_m]_s$ laminates asymptotically approach the value of 1 from above as the number of plies increases. The values of β and $(D_{11}/D_{22})^{1/4}$ for the $[(0/90/\pm45)_m]_s$ laminates asymptotically approach the value of 1 from above and below, respectively, as the number of plies increases. A value of 1 for β and $(D_{11}/D_{22})^{1/4}$ and a value of 0 for γ and δ represent pure isotropy associated with a plate made from an essentially homogeneous material like wrought aluminum plate.

The results presented in figure 5 for the $[(\pm45/0_2)_m]_s$ and $[(\pm45/90_2)_m]_s$ laminates indicate that anisotropic parameters γ and δ also asymptotically approach zero from above as the number of plies increases. The solid curves and dashed curves shown in figure 5 indicate results for the $[(\pm45/0_2)_m]_s$ and $[(\pm45/90_2)_m]_s$ laminates, respectively. The results in figure 5 indicate that both laminate families have the same value of the orthotropic parameter β for a given number of plies, and that β decreases monotonically to an asymptotic value as the number of plies increases. In contrast, the $[(\pm45/0_2)_m]_s$ laminates have larger values of $(D_{11}/D_{22})^{1/4}$ than the $[(\pm45/90_2)_m]_s$ laminates. Moreover, the values of $(D_{11}/D_{22})^{1/4}$ for the $[(\pm45/90_2)_m]_s$ and $[(\pm45/0_2)_m]_s$ laminates monotonically diminish and increase, respectively, as the number of plies increases.

Effects of Varying Material Properties

Results showing the effects of varying material properties on the nondimensional parameters for $[\pm\theta]_s$ angle-ply laminates are presented in figures 6 through 9. In these figures, results are presented for laminates made of high-strength graphite-epoxy material, ultrahigh-modulus graphite-epoxy material, S-glass-epoxy material, Kevlar-epoxy material, boron-epoxy material, and boron-aluminum material. The moduli ratios E_1/E_2 and E_2/G_{12} and the major Poisson's ratio ν_{12} for these materials are given in table 1.

Table 1. Stiffness Ratios and Major Poisson's Ratio for Common Lamina Material Systems

Material system	$\frac{E_1}{E_2}$	$\frac{E_2}{G_{12}}$	ν_{12}
High-strength graphite-epoxy	11.6	1.9	0.35
Kevlar-epoxy	13.8	2.7	0.34
S-glass-epoxy	4.4	2.1	0.25
Ultrahigh-modulus graphite-epoxy	50.0	1.5	0.26
Boron-epoxy	10.0	4.3	0.21
Boron-aluminum	1.6	3.0	0.23

The results presented in figure 6 show that maximum values of the orthotropic parameter β occur at $\theta = 45°$ for all the material properties considered. The largest values of β are, for most of the range of fiber orientation angles, exhibited by laminates made of ultrahigh-modulus graphite-epoxy material; these are followed by laminates made of Kevlar-epoxy material, boron-epoxy material, high-strength graphite-epoxy material, S-glass-epoxy material, and boron-aluminum material. The results presented in figure 7 indicate that the largest value of $(D_{11}/D_{22})^{1/4}$ is also exhibited by laminates made of ultrahigh-modulus graphite-epoxy material for $0° \leq \theta \leq 45°$. The next highest values of $(D_{11}/D_{22})^{1/4}$ in the range of $0° \leq \theta \leq 45°$ are exhibited by laminates made of Kevlar-epoxy material, high-strength graphite-epoxy material, boron-epoxy material, S-glass-epoxy material, and boron-aluminum material. In the range of $45° \leq \theta \leq 90°$, the trend reverses.

The results presented in figures 8 and 9 indicate that the largest values for the anisotropic parameters γ and δ are also exhibited by laminates made of ultrahigh-modulus graphite-epoxy material followed by laminates made of Kevlar-epoxy material, boron-epoxy material, high-strength graphite-epoxy material, S-glass-epoxy material, and boron-aluminum material, i.e., the same trend as that exhibited by the orthotropic parameter β. The maximum values of γ and δ for each material system range for θ between 31° and 59°. For example, γ is at a maximum at $\theta = 31°$ ($\gamma = 0.13$) and δ is at a maximum at $\theta = 59°$ ($\delta = 0.13$) for laminates made of boron-aluminum material. For laminates made of ultrahigh-modulus graphite-epoxy material, γ is at a maximum at $\theta = 40°$ ($\gamma = 0.68$), and δ is at a maximum at $\theta = 50°$ ($\gamma = 0.68$).

The results discussed in this section indicate a practical range of the numerical values of the nondimensional parameters. In subsequent sections of this paper, generic buckling results are presented for

the ranges of $0.2 \leq \beta \leq 3.0$, $0.5 \leq (D_{11}/D_{22})^{1/4} \leq 3.0$, $0 \leq \gamma \leq 0.8$, and $0 \leq \delta \leq 0.8$. Negative values for γ and δ are possible for some laminates (e.g., $[\mp 45]_s$ laminates), but they are not considered in the present paper. An important physical consideration to keep in mind when using the nondimensional parameters in an arbitrary manner to generate buckling design charts is that together they must satisfy the condition that the strain energy of the plate have a positive value. This condition is due to the thermodynamic restrictions that define the admissible range of lamina material properties, and hence define the range of admissible plate bending stiffnesses. This condition was enforced in the buckling analysis and accounts for the fact that some of the curves shown on the generic buckling design charts presented herein do not span the entire range of the nondimensional parameters specified herein.

Buckling Results and Discussion

Results are presented in this section for clamped and simply supported plates loaded by either axial compression or shear. In addition, results are presented for plates subjected to a combined loading of axial tension or compression and shear, transverse tension or compression and shear, and transverse tension or compression and axial compression. In each of the loading cases involving shear, a distinction between positive and negative shear loadings is made whenever anisotropy is present. A positive shear loading corresponds to a shear stress acting on the plate edge $y = b$ (see fig. 1) in the positive x-coordinate direction. For each of the loading cases considered in the present paper, results are first presented for the familiar angle-ply laminates, and then generic results are presented in terms of the nondimensional parameters described herein. The results presented for the angle-ply laminates are calculated using lamina material properties of a typical graphite-epoxy material. The properties used are the same ones that were used to calculate the nondimensional parameters shown in figure 2.

Axial-Compression-Loaded Plates

Nondimensional buckling coefficients K_x as a function of the fiber orientation angle θ are presented in figure 10 for infinitely long, clamped and simply supported $[\pm\theta]_s$ plates loaded in axial compression. The 4-ply $[\pm\theta]_s$ laminates are limiting cases, but they are useful in the present study since they exhibit the highest degree of anisotropy of the angle-ply laminates. Similar results are presented in figure 11 for $[(\pm 45)_m]_s$ plates for $m = 1, 2, \ldots, 12$. The solid curves shown in figures 10 and 11 correspond to results for which anisotropy is included in the analysis. The dashed curves in the figures correspond to results for which the D_{16} and D_{26} anisotropic constitutive terms are neglected. The buckling coefficients shown in figure 10 were calculated for increments in θ equal to 1°. Similar sets of results for square finite-length plates are presented in reference 1.

The results presented in figure 10 indicate that neglecting plate anisotropy in the analysis always overestimates the plate bending stiffness, and thus always yields nonconservative estimates of the buckling resistance. The largest buckling coefficients for the orthotropic plates occur at $\theta = 45°$, whereas the largest ones for the anisotropic plates occur at slightly less than 45°. The largest difference between the orthotropic and anisotropic solutions for both clamped and simply supported plates is about 25 percent of the corresponding orthotropic solution.

The results presented in figure 11 indicate that the anisotropic solutions for both clamped and simply supported plates converge monotonically from below to the specially orthotropic solutions as the number of plies in the $[(\pm 45)_m]_s$ laminates increases. The largest difference between the anisotropic and orthotropic solutions occurs for $m = 1$ and is approximately 25 percent of the corresponding orthotropic solution. The difference is approximately 5 percent for $m = 2$ and less than 1 percent for $m = 6$.

Generic buckling results for clamped compression-loaded plates are presented in figures 12 through 14 for a wide range of values of the four nondimensional parameters. The results presented in figure 12 show buckling coefficients of clamped plates as a function of the parameter $(D_{11}/D_{22})^{1/4}$ for $\beta = 3$. Buckling curves are presented in this figure for discrete values of $\gamma = \delta$ ranging from 0 to 0.8. The $[\pm 45]_s$ laminates made of a typical graphite-epoxy material and an ultrahigh-modulus graphite-epoxy material have values of γ and δ equal to 0.52 and 0.68, respectively. Thus, a value of 0.8 corresponds to an extremely anisotropic plate. The straight lines shown in figure 12 are parallel to the abscissa axis and thus indicate that the buckling coefficients are independent of the parameter $(D_{11}/D_{22})^{1/4}$ for the entire range of anisotropy shown in the figure.

Similar plots were made for clamped and simply supported plates in which the orthotropic parameter β was varied and unequal values of γ and δ were used. The additional results also show the buckling coefficients to be independent of the parameter $(D_{11}/D_{22})^{1/4}$. This finding is consistent with the observation that plots of buckling coefficient versus plate aspect ratio (length over width) for finite-length plates attenuate to constant values

as the plate aspect ratio becomes large. More specifically, in a finite-length plate the bending stiffness ratio $(D_{11}/D_{22})^{1/4}$ influences the size and number of buckles that occur along the plate length. The number of buckles that occur along the plate length, in turn, directly affects the value of the buckling coefficient for a given plate (as indicated by the festoon nature of the buckling curves for finite-length plates). For an infinitely long plate, the bending stiffness ratio $(D_{11}/D_{22})^{1/4}$ still influences the size of the buckles with respect to the basic periodic unit of an infinitely long plate, but the number of buckles that occur along the plate length becomes meaningless.

The independence of K_x with respect to $(D_{11}/D_{22})^{1/4}$ represents an important simplification in that the buckling coefficients of long plates can be represented by a single orthotropic parameter, namely, β. However, the parameter $(D_{11}/D_{22})^{1/4}$ is important since it does affect the aspect ratio of the buckle pattern, and it is useful in determining when classical plate theory becomes insufficient and transverse shear deformation must be included in buckling analyses.

Buckling coefficients are presented in figure 13 for clamped compression-loaded plates as a function of the orthotropic parameter β for values of $\gamma = \delta$ ranging from 0 to 0.8. Using the result that the buckling coefficients are independent of $(D_{11}/D_{22})^{1/4}$, results corresponding to particular laminates made of a typical graphite-epoxy material and an ultrahigh-modulus graphite-epoxy material are also shown in figure 13 and are indicated by symbols. The symbols that represent several laminates indicate that all the laminates have the same buckling coefficient. The results presented in this figure indicate that anisotropy can significantly reduce buckling resistance and that the effect of anisotropy tends to diminish somewhat as β increases (i.e., the curves become spaced closer together as β increases). Similar results were obtained for simply supported plates. These results indicate the same trends and indicate that the effects of varying β are slightly more pronounced for the clamped plates. (That is, the linear portions of the curves for the clamped plates generally had a higher slope than the corresponding curves for the simply supported plates.)

Results are presented in figure 14 for clamped compression-loaded plates in which the anisotropic parameters γ and δ are varied independently. Curves are also presented in this figure for values of γ and δ ranging from 0 to 0.8. Moreover, two sets of curves are shown in figure 14 corresponding to values of the orthotropic parameter β equal to 1 and 3. The results presented in this figure indicate that the buckling coefficients are more sensitive to the parameter δ than to γ. This observation can be seen by comparing the differences in the values of the buckling coefficients in which γ is held constant and δ is varied, and vice versa. The results also support the previous statement that the effect of anisotropy tends to diminish somewhat as β increases. A set of results similar to those presented in figure 14 were obtained for simply supported plates. These results indicate the same trends and indicate that the effects of varying β, γ, and δ are also slightly more pronounced for the clamped plates.

Shear-Loaded Plates

Shear buckling coefficients K_s are presented in figure 15 as a function of the fiber orientation angle θ for infinitely long, clamped and simply supported $[\pm\theta]_s$ plates. Similar results are presented in figure 16 for $[(\pm 45)_m]_s$ plates for $m = 1, 2, \ldots, 12$. The solid and dotted curves shown in figures 15 and 16 correspond to results for which anisotropy is included in the analysis. The solid curves correspond to a positive shear loading, and the dotted curves correspond to a negative shear loading. The dashed curves in the figures correspond to results for which anisotropy is neglected, and no distinction between positive and negative shear is necessary. The buckling coefficients shown in figure 15 were calculated for increments in θ equal to 1°.

The results presented in figure 15 indicate that neglecting plate anisotropy in the analysis yields nonconservative estimates of the buckling resistance of plates loaded in positive shear and conservative estimates for the plates loaded in negative shear. Moreover, the plates loaded in negative shear exhibit the most buckling resistance. The largest buckling coefficients occur at $\theta = 45°$ for the orthotropic plates and at slightly more than 45° for the anisotropic plates loaded in negative shear. The largest buckling coefficients occur at $\theta = 0°$ and 90° for the clamped plates loaded in positive shear and at 20° for the corresponding simply supported plates. The largest difference between the orthotropic and anisotropic solutions for both clamped and simply supported plates is approximately 48 percent of the corresponding orthotropic solution. This difference is nearly twice that of the corresponding compression-loaded plates.

The results presented in figure 16 indicate that the anisotropic solutions for both clamped and simply supported plates converge monotonically to the specially orthotropic solutions as the number of plies increases in the $[(\pm 45)_m]_s$ laminates. The plates loaded by negative shear converge from above, and

the plates loaded by positive shear converge from below. The largest difference between the anisotropic and orthotropic solutions occurs for $m = 1$ and is approximately 48 percent of the corresponding orthotropic solution. The difference is approximately 7 percent for $m = 6$ and approximately 3.5 percent for $m = 12$. Comparing the results presented in figures 11 and 16 indicates that the effects of anisotropy are much more pronounced in shear-loaded plates than in compression-loaded plates.

Generic buckling results for clamped and simply supported shear-loaded plates are presented in figures 17 through 19 for a wide range of values of the nondimensional parameters. The results presented in figure 17 show buckling coefficients of clamped plates as a function of the parameter $(D_{11}/D_{22})^{1/4}$ for $\beta = 3$. Buckling curves are presented in this figure for values of $\gamma = \delta$ ranging from 0 to 0.8. Like the compression-loaded plates, the results presented in figure 17 indicate that the buckling coefficients are independent of the parameter $(D_{11}/D_{22})^{1/4}$ for the entire range of anisotropy. Similar results were obtained for clamped and simply supported plates in which the orthotropic parameter β was varied. The additional results also show that the buckling coefficients are independent of the parameter $(D_{11}/D_{22})^{1/4}$. The parameter $(D_{11}/D_{22})^{1/4}$ was found, however, to affect the aspect ratio of the buckle pattern.

Buckling coefficients are presented in figure 18 for clamped shear-loaded plates as a function of the orthotropic parameter β. Curves are also presented in this figure for values of $\gamma = \delta$ ranging from 0 to 0.8. Since the buckling coefficients are independent of $(D_{11}/D_{22})^{1/4}$, the results corresponding to particular laminates that are made of a typical graphite-epoxy material and an ultrahigh-modulus graphite-epoxy material are indicated in the figure by symbols. Like the compression-loaded plates, the results presented in this figure indicate that anisotropy can significantly reduce buckling resistance of shear-loaded plates and that the effects of anisotropy tend to diminish somewhat as β increases. Similar results were obtained for simply supported plates. These results also indicate the same trends and demonstrate that the effects of varying β are slightly more pronounced for the clamped plates.

Results are presented in figure 19 for clamped shear-loaded plates as a function of the anisotropic parameters γ and δ with values ranging from 0 to 0.8 for $\beta = 3$. The results presented in figure 19 indicate the same trend shown in figure 14 for the compression-loaded plates; i.e., the buckling coefficients are more sensitive to δ than to γ. Similar results were obtained for $\beta = 1$. These results also indicate that the effects of anisotropy tend to diminish somewhat as β increases. Results similar to those presented in figure 19 were obtained for simply supported plates with $\beta = 1$ and 3. These results indicate the same trends and once again reveal that the effects of varying β, γ, and δ are slightly more pronounced for the clamped plates than for the simply supported plates.

Plates Subjected to Combined Loadings

Results are presented in this section for plates subjected to combined loadings. First, results are presented for plates subjected to axial tension or compression loadings combined with shear loading. Next, results are presented for plates subjected to transverse tension or compression loadings combined with shear loading. Last, results are presented for plates subjected to axial compression combined with either transverse tension or compression loadings.

Axial tension or compression loadings combined with shear loading. Buckling interaction curves are presented in figure 20 for infinitely long clamped $[\pm\theta]_s$ plates subjected to axial tension or compression and shear loadings for several fiber orientation angles θ. The dashed curves shown in figure 20 correspond to results for which anisotropy is included in the analysis, and the solid curves correspond to results for which the D_{16} and D_{26} anisotropic constitutive terms are neglected. Negative values of K_x correspond to axial tension loadings, and negative values of K_s correspond to negative shear loadings. Points of intersection of the interaction curves shown in figure 20 with a straight line emanating from the origin of the plot constitute constant values of $(N_{xy}/N_x)\,(D_{11}/D_{22})^{1/4}$ and are depicted in the figure for convenience.

The results presented in figure 20 indicate that the effects of anisotropy manifest themselves as a phase shift of self-similar curves in the K_xK_s-plane. The self-similar nature of the curves suggests that it may be possible to obtain simple buckling interaction formulas like those existing for isotropic plates. (See ref. 5.) For plates loaded in positive shear, neglecting plate anisotropy in an analysis yields buckling coefficients substantially larger than those corresponding to the anisotropic solution. For plates loaded in negative shear, however, this trend is reversed. Similar results were obtained for corresponding simply supported plates, and these results exhibit exactly the same trends. In addition, both the results in

figure 20 and the corresponding results for simply supported plates suggest that the buckling resistance of a compression-loaded plate can be improved by applying a negative shear loading. For the plates with $\theta = 45°$, the improvement is approximately 20 percent and 25 percent of the K_x values corresponding to pure axial compression loading for the clamped and simply supported plates, respectively. The results presented in figure 20 also indicate that laminates with $\theta = 45°$ yield the most buckling-resistant interaction curves for both cases in which anisotropy is included and neglected. This trend is also exhibited by the simply supported plates.

Generic buckling results for clamped and simply supported plates subjected to combined axial and shear loadings are also presented in figures 21 through 23 for a wide range of values of the nondimensional parameters. Additional results were obtained for both boundary condition cases and several values of β, γ, and δ. These additional results indicate that the buckling interaction curves, such as those presented in figures 21 through 23, are independent of the parameter $(D_{11}/D_{22})^{1/4}$.

Buckling interaction curves are presented in figure 21 for clamped and simply supported plates and for several values of the orthotropic parameter β. The curves appearing in this figure are for values of $\gamma = \delta = 0$. By using the simplification that the buckling interaction curves are independent of $(D_{11}/D_{22})^{1/4}$, results corresponding to particular laminates can be obtained once the value of β for the specific laminate is known, provided the corresponding nondimensional anisotropic parameters have a value of zero. Good estimates of buckling resistance can be otained for laminates with small values of the nondimensional anisotropic parameters compared to unity. For example, the curves with $\beta = 1$ correspond to solutions for isotropic plates and give good approximations to the results for $[(\pm 45/0/90)_m]_s$ quasi-isotropic laminates with 32 or more plies made of a typical graphite-epoxy material. An important result shown in figure 21 is that substantial gains in buckling resistance can be obtained by tailoring laminate construction to increase the parameter β.

Results are presented in figure 22 for clamped and simply supported plates with values of $\gamma = \delta$ ranging from 0 to 0.8 and for $\beta = 3$. These results also show that anisotropy is generally manifested as a phase shift of the interaction curves in the $K_x K_s$-plane. The results in figure 22 support the statement given previously that the buckling resistance of a compression-loaded plate can be improved by applying a negative shear loading (as was seen for the angle-ply laminates). For extremely anisotropic plates with $\gamma = \delta = 0.8$, the improvement indicated by these results is approximately 90 percent and 85 percent of the K_x values corresponding to pure compression loading for the clamped and simply supported plates, respectively. The results presented in figure 22 also indicate that plates with $\gamma = \delta = 0$ are the most buckling resistant of the plates loaded by positive shear forces, whereas the plates with $\gamma = \delta = 0.8$ are the most buckling resistant of the plates loaded by negative shear forces. This trend is also exhibited by the simply supported plates.

Results are presented in figure 23 for clamped plates with $\beta = 1$ as a function of the anisotropic parameters γ and δ. Curves are shown in this figure for values of $\gamma = 0$ and 0.4 and for values of δ ranging from 0 to 0.6. The results presented in figure 23 indicate the same trend as that shown in figure 14 for the axial compression-loaded plates and in figure 19 for the shear-loaded plates; i.e., the buckling coefficients are more sensitive to the anisotropic parameter δ than to γ.

Transverse tension or compression loadings combined with shear loading. Buckling interaction curves are presented in figure 24 for infinitely long clamped $[\pm\theta]_s$ plates subjected to transverse tension or compression and shear loadings for several fiber orientation angles θ. The dashed curves shown in figure 24 correspond to results for which anisotropy is included, and the solid curves correspond to solutions for which it is neglected. Negative values of K_y correspond to transverse tension loadings, and negative values of K_s correspond to negative shear loadings. Points of intersection of the interaction curves shown in figure 24 with a straight line emanating from the origin of the plot constitute constant values of $(N_y/N_{xy})\,(D_{11}/D_{22})^{1/4}$. The horizontal straight-line portions of the buckling interaction curves indicate values of the buckling coefficients for which a plate buckles into a wide column mode ($K_y = 4$ for clamped plates). For this mode, the half-wavelength λ shown in figure 1 approaches infinity in the analysis.

The results presented in figure 24 indicate that the effects of anisotropy also manifest themselves as a phase shift of self-similar curves in the $K_s K_y$-plane for these loading conditions. For plates loaded in positive shear, neglecting plate anisotropy in an analysis yields buckling coefficients substantially larger than those corresponding to the anisotropic solution. In addition, the value of K_s at which the

plate buckles into a wide column mode is significantly overestimated. For plates loaded in negative shear, this trend is reversed. The coalescence of all the curves shown in figure 24 into the same horizontal-line segment at $K_y = 4$ indicates that anisotropy is unimportant for plates that buckle into a wide column mode; i.e., the transverse loading N_y forces the plate to assume a deformation state that is not skewed (or it is skewed at $x = \pm\infty$). Similar results were obtained for corresponding simply supported plates, and these results exhibit exactly the same trends. The simply supported plates buckle into a wide column mode at $K_y = 1$.

Generic buckling results for clamped and simply supported plates subjected to combined axial and shear loadings are presented in figures 25 through 27. Additional results were obtained for both boundary condition cases and several values of β, γ, and δ. These additional results indicate that the buckling interaction curves for this combination of loadings are also independent of the parameter $(D_{11}/D_{22})^{1/4}$.

Buckling interaction curves are presented in figure 25 for clamped and simply supported plates with several values of the orthotropic parameter β and with $\gamma = \delta = 0$. Once again, the fact that the buckling interaction curves are independent of $(D_{11}/D_{22})^{1/4}$ permits results for particular laminates with zero-valued (or small compared to unity) anisotropic parameters to be obtained directly from figure 25 once the value of β for the specific laminate is known. The results shown in figure 25 indicate that substantial gains in buckling resistance can be obtained by tailoring laminate construction to increase the parameter β.

Generic buckling results are presented in figure 26 for clamped and simply supported plates with values of $\gamma = \delta$ ranging from 0 to 0.8 and for a value of $\beta = 3$. These results also confirm the results presented in figure 24 that show that the anisotropy is generally manifested as a phase shift of the interaction curves in the $K_s K_y$-plane, and that anisotropy does not affect the wide column buckling mode. The results presented in figure 26 also indicate that plates with $\gamma = \delta = 0$ are the most buckling resistant of the plates loaded by positive shear forces, whereas the plates with $\gamma = \delta = 0.8$ are the most buckling resistant of the plates loaded by negative shear forces.

Results are presented in figure 27 for clamped plates with $\beta = 3$ in which the anisotropic parameters γ and δ are varied independently. Buckling interaction curves are shown in this figure for $\gamma = 0$ and 0.6 and for values of δ ranging from 0 to 0.6. The results presented in figure 27 indicate that the plates loaded by transverse tension or compression and shear are also more sensitive to the anisotropic parameter δ than to γ.

Axial compression combined with either transverse tension loading or compression loading. Buckling interaction curves are presented in figure 28 for infinitely long, clamped and simply supported $[\pm\theta]_s$ plates subjected to transverse tension or compression and axial compression loadings for several fiber orientation angles θ. The dashed curves shown in figure 28 correspond to results for which anisotropy is included in the analysis, and the solid curves correspond to results for which it is neglected. In this figure the points of intersection of the interaction curves with a straight line emanating from the origin of the plot constitute constant values of $(N_y/N_x)\,(D_{11}/D_{22})^{1/2}$. The horizontal straight-line portions of the buckling interaction curves indicate values of the buckling coefficients at which a plate buckles into a wide column mode.

The results presented in figure 28 indicate that the effects of anisotropy for plates subjected to these loading conditions also generally manifest themselves as a phase shift of self-similar curves in the $K_x K_y$-plane. Neglecting plate anisotropy in an analysis always yields buckling coefficients larger than those corresponding to the anisotropic solution. Similar to the plates loaded by shear and transverse compression, the value of K_x at which the plate buckles into a wide column mode is substantially overestimated when anisotropy is neglected.

Generic buckling results are presented in figures 29 through 31 for clamped and simply supported plates subjected to combined axial and transverse loadings. Additional results were obtained for both boundary condition cases and several values of β, γ, and δ. These additional results indicate that the buckling interaction curves for this combination of loadings are also independent of the parameter $(D_{11}/D_{22})^{1/4}$.

Buckling interaction curves are presented in figure 29 for clamped and simply supported plates with several values of the orthotropic parameter β and with $\gamma = \delta = 0$. Since the buckling interaction curves are independent of $(D_{11}/D_{22})^{1/4}$, results for particular laminates with zero-valued (or small compared to unity) nondimensional anisotropic parameters can be obtained directly from figure 29 once the value of β for the specific laminate is known. The results shown in figure 29 indicate that substantial gains in buckling resistance can be obtained when β increases.

Generic buckling results are presented in figure 30 for clamped plates with values of $\gamma = \delta$ ranging from 0 to 0.6. Two sets of curves are shown in the figure. The solid and dashed curves correspond to values of $\beta = 3$ and 1, respectively. These results also show a phase shift due to anisotropy, and they show that the effects of anisotropy are more pronounced for plates with $\beta = 1$ than for plates with $\beta = 3$. The results presented in figure 30 also indicate that plates with $\gamma = \delta = 0$ are the most buckling resistant of the plates when nonzero axial loading is present.

Results are presented in figure 31 for clamped plates with $\beta = 3$ as a function of the anisotropic parameters γ and δ. Curves are shown in this figure for $\gamma = 0$ and 0.6 and for values of δ ranging from 0 to 0.6. The results presented in figure 31 indicate that the plates loaded by transverse tension or compression and axial compression are also generally more sensitive to the parameter δ than to γ.

Concluding Remarks

A parametric study has been presented of the buckling behavior of infinitely long, symmetrically laminated anisotropic plates subjected to combined loadings. Loading conditions consisting of axial tension and compression, transverse tension and compression, and shear were investigated for clamped and simply supported plates. Results are presented that were obtained using a special-purpose analysis that was derived in terms of useful nondimensional parameters. The analysis was found to be well-suited for parametric studies. Buckling results are also presented for some common laminate constructions, and generic buckling design charts have been presented for a wide range of parameters. The generic design charts are presented in terms of useful nondimensional parameters, and the dependence of the nondimensional parameters on laminate fiber orientation, stacking sequence, and material properties is discussed.

The results presented in the present paper show that nondimensional parameters can be very useful in presenting results in a concise manner for a wide range of loading conditions, boundary conditions, and laminate constructions. Results are presented that show that the effects of anisotropy are much more pronounced in shear-loaded plates than in compression-loaded plates. In addition, the effects of anisotropy on plates subjected to combined loadings are shown to be generally manifested as phase shifts of self-similar buckling interaction curves. These results indicate that the buckling resistance of long compression-loaded, highly anisotropic plates can be improved significantly by applying a shear loading with a specific orientation. Moreover, it is shown that anisotropy reduces the buckling resistance of biaxially compressed plates.

A substantial number of generic buckling results are presented in the present paper for a wide range of values of the nondimensional parameters. In all cases considered in the study, the buckling coefficients of infinitely long plates are shown to be independent of the bending stiffness ratio $(D_{11}/D_{22})^{1/4}$. Also, large increases in buckling resistance are shown to be obtained by tailoring the laminate construction to increase the parameter $\beta = (D_{12} + 2D_{66})/(D_{11}D_{22})^{1/2}$, and the importance of anisotropy generally diminishes as β increases. Results are also presented that show the buckling coefficients to be generally more sensitive to the anisotropic parameter $\delta = D_{26}/(D_{11}D_{22}^3)^{1/4}$ than to the anisotropic parameter $\gamma = D_{16}/(D_{11}^3 D_{22})^{1/4}$ for the entire range of loadings and boundary conditions considered.

NASA Langley Research Center
Hampton, VA 23665-5225
March 25, 1992

References

1. Nemeth, Michael P.: Importance of Anisotropy on Buckling of Compression-Loaded Symmetric Composite Plates. *AIAA J.*, vol. 24, no. 11, Nov. 1986, pp. 1831–1835.

2. Grenestedt, Joachim L.: A Study on the Effect of Bending-Twisting Coupling on Buckling Strength. *Compos. Struct.*, vol. 12, no. 4, 1989, pp. 271–290.

3. Johns, D. J.: *Shear Buckling of Isotropic and Orthotropic Plates—A Review.* R. & M. No. 3677, British Aeronautical Research Council, 1971.

4. Stein, Manuel: Postbuckling of Orthotropic Composite Plates Loaded in Compression. *A Collection of Technical Papers—23rd Structures, Structural Dynamics and Materials Conference, Part 1—Structures and Materials*, May 1982, pp. 479–486. (Available as AIAA-82-0778.)

5. Gerard, George; and Becker, Herbert: *Handbook of Structural Stability. Part I—Buckling of Flat Plates.* NACA TN 3781, 1957.

6. Stowell, Elbridge Z.: *Critical Shear Stress of an Infinitely Long Flat Plate With Equal Elastic Restraints Against Rotation Along the Parallel Edges.* NACA WR L-476, 1943. (Formerly NACA ARR 3K12.)

7. Stowell, Elbridge Z.; and Schwartz, Edward B.: *Critical Stress for an Infinitely Long Flat Plate With Elastically Restrained Edges Under Combined Shear and*

Direct Stress. NACA WR L-340, 1943. (Formerly NACA ARR 3K13.)

8. Batdorf, S. B.; and Houbolt, John C.: *Critical Combinations of Shear and Transverse Direct Stress for an Infinitely Long Flat Plate With Edges Elastically Restrained Against Rotation.* NACA Rep. 847, 1946. (Formerly NACA ARR L4L14.)

9. Batdorf, S. B.; Stein, Manuel; and Libove, Charles: *Critical Combinations of Longitudinal and Transverse Direct Stress for an Infinitely Long Flat Plate With Edges Elastically Restrained Against Rotation.* NACA WR L-49, 1946. (Formerly NACA ARR L6A05a, 1946.)

10. Housner, Jerrold M.; and Stein, Manuel: *Numerical Analysis and Parametric Studies of the Buckling of Composite Orthotropic Compression and Shear Panels.* NASA TN D-7996, 1975.

11. Wittrick, W. H.; and Williams, F. W.: Buckling and Vibration of Anisotropic or Isotropic Plate Assemblies Under Combined Loadings. *Int. J. Mech. Sci.*, vol. 16, no. 4, Apr. 1974, pp. 209–239.

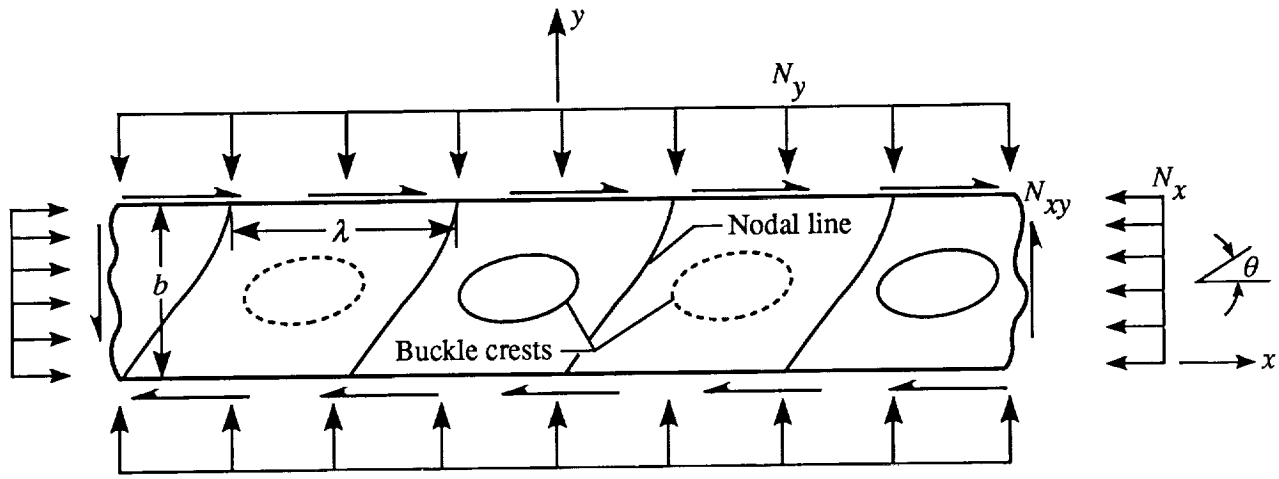

Figure 1. Geometry of buckled plate subjected to biaxial compression and shear loadings.

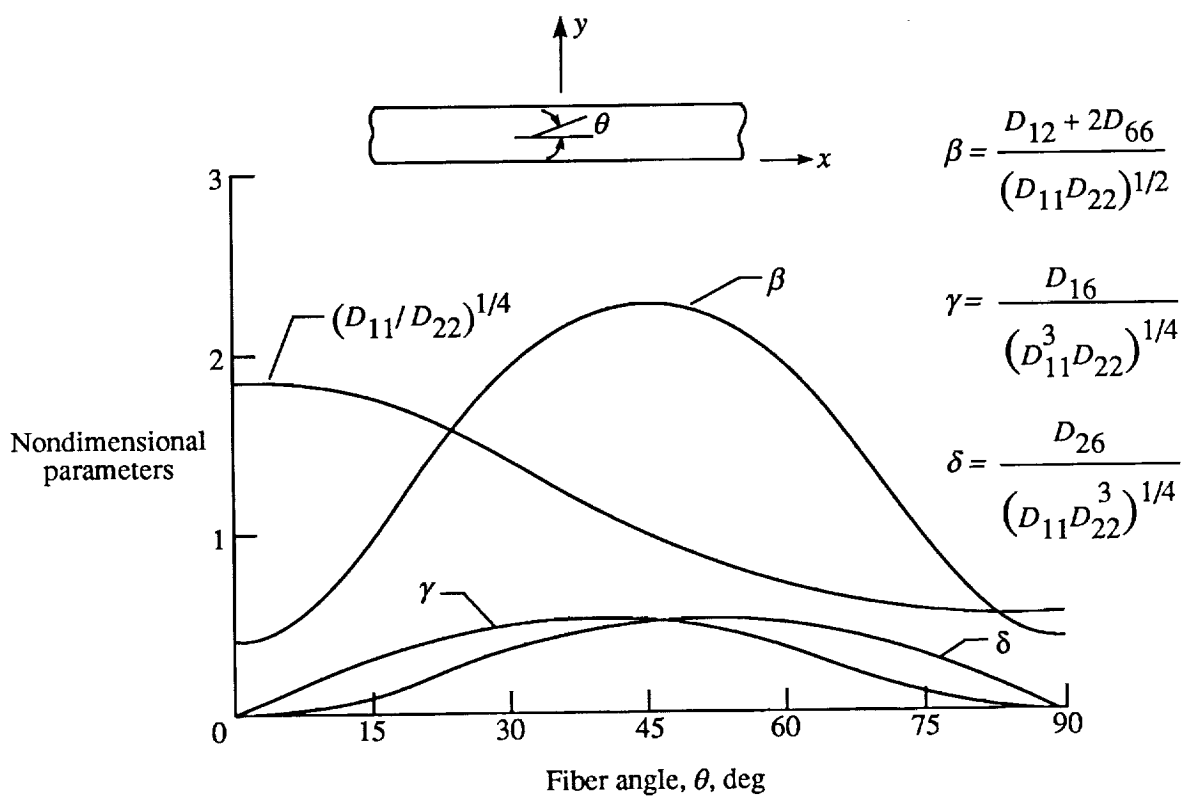

Figure 2. Nondimensional parameters for $[\pm\theta]_s$ graphite-epoxy laminates.

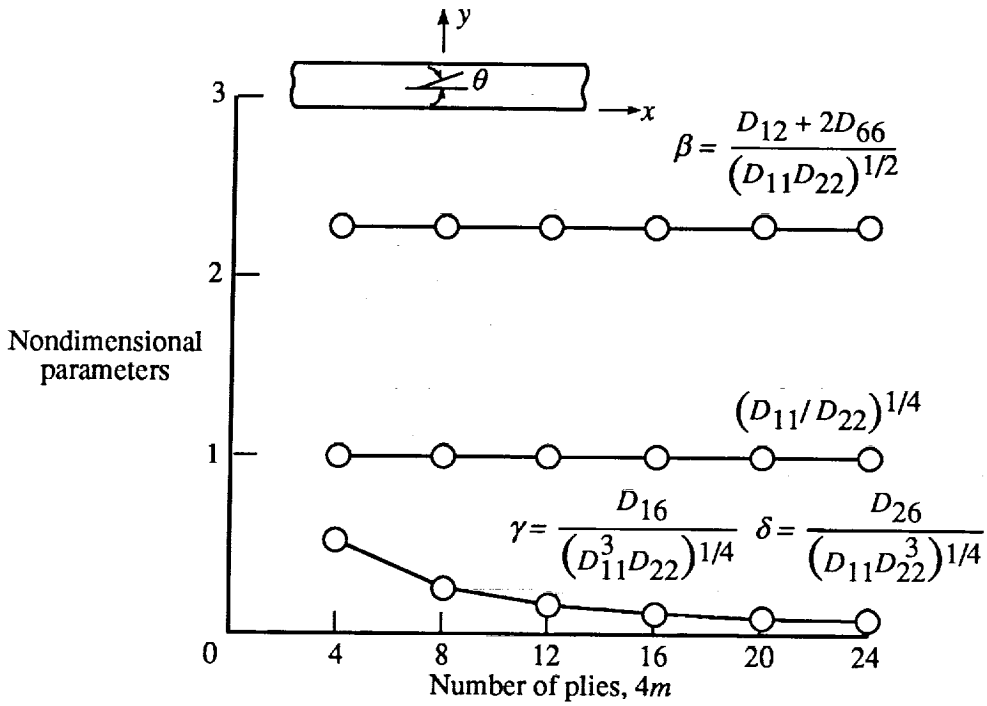

Figure 3. Nondimensional parameters for $[(\pm 45)_m]_s$ graphite-epoxy laminates.

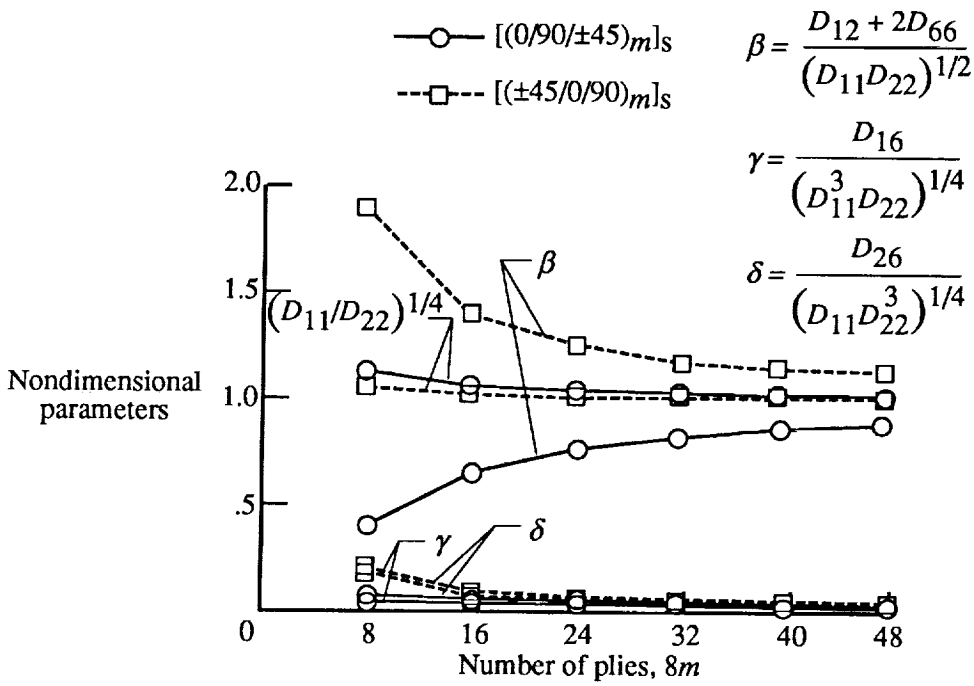

Figure 4. Nondimensional parameters for quasi-isotropic graphite-epoxy laminates.

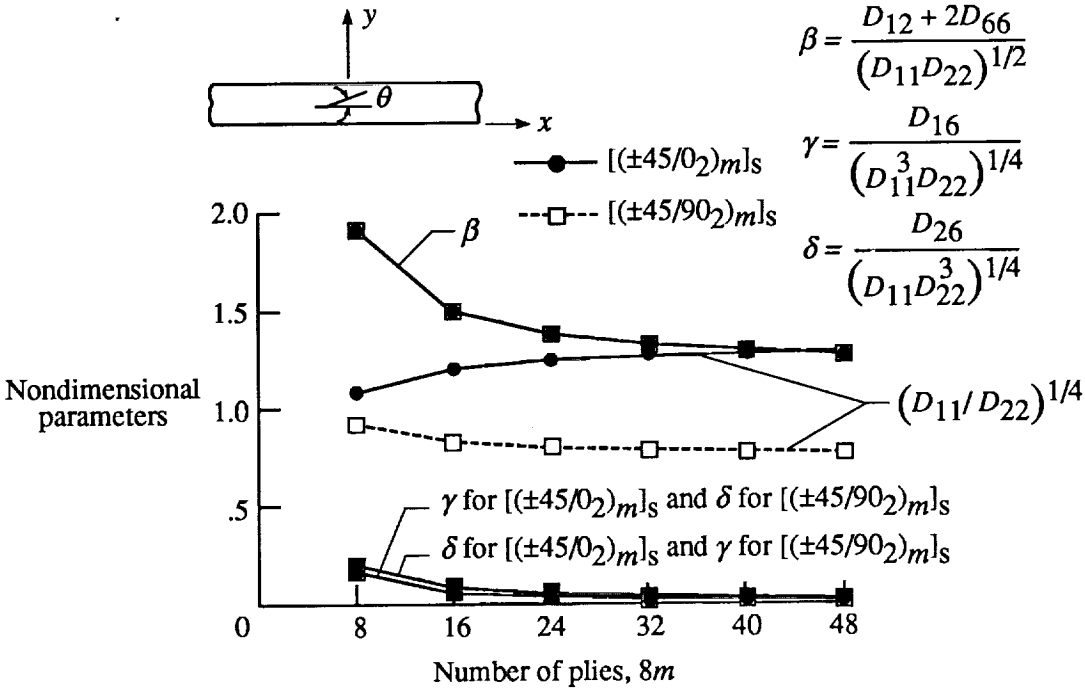

Figure 5. Nondimensional parameters for $[(\pm 45/0_2)_m]_s$ and $[(\pm 45/90_2)_m]_s$ graphite-epoxy laminates.

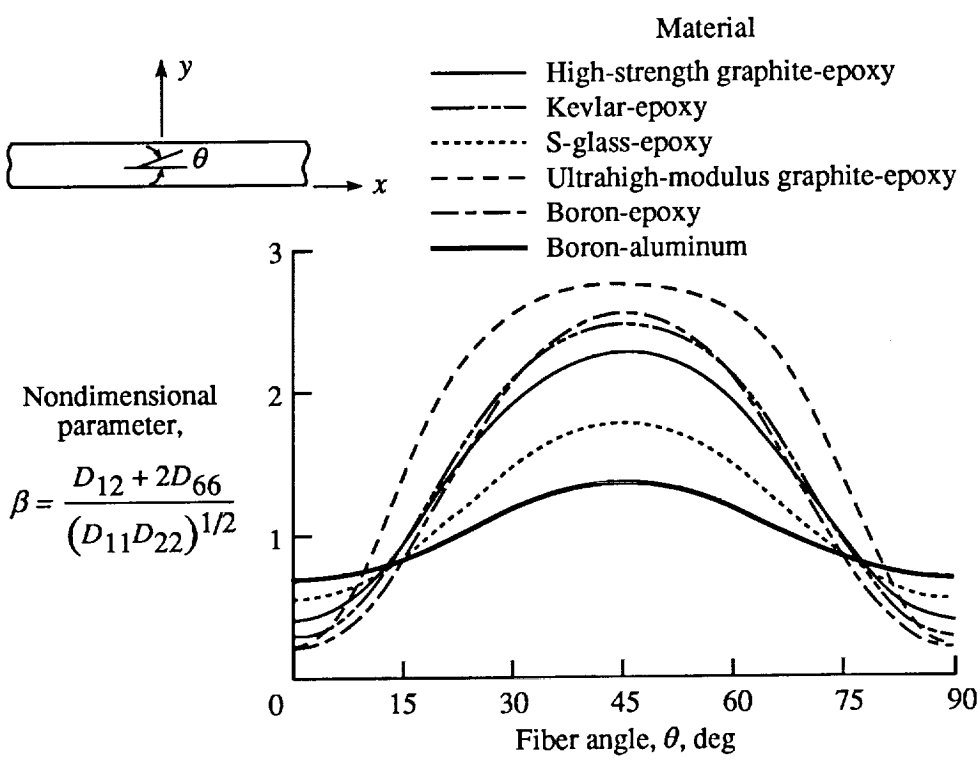

Figure 6. Effect of lamina material properties on nondimensional orthotropic parameter β for $[\pm\theta]_s$ laminates.

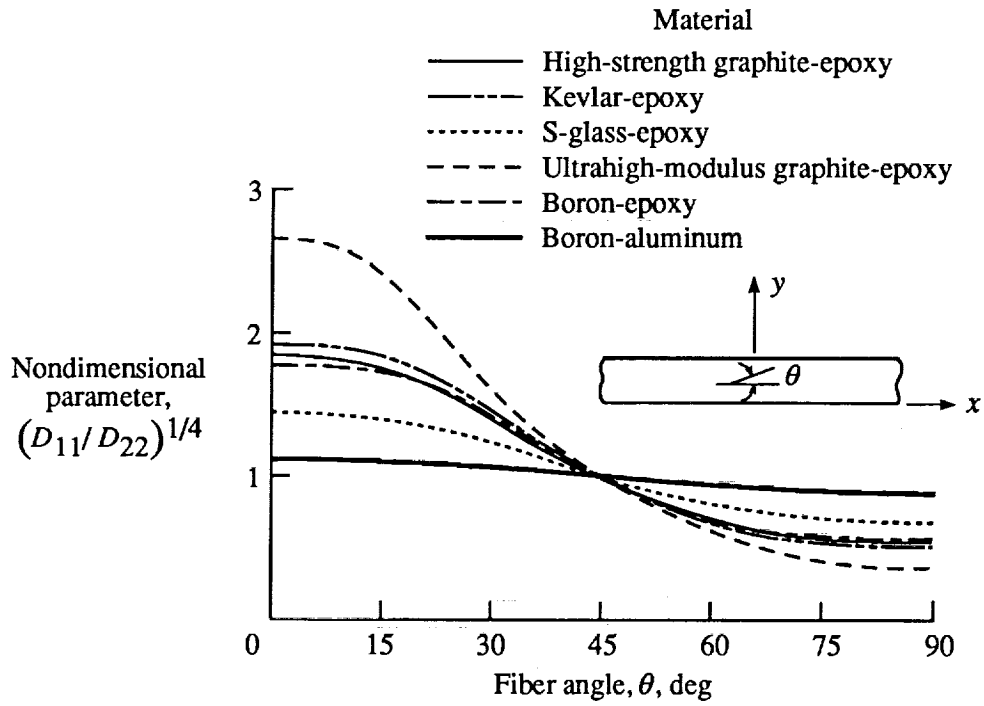

Figure 7. Effect of lamina material properties on parameter $(D_{11}/D_{22})^{1/4}$ for $[\pm\theta]_s$ laminates.

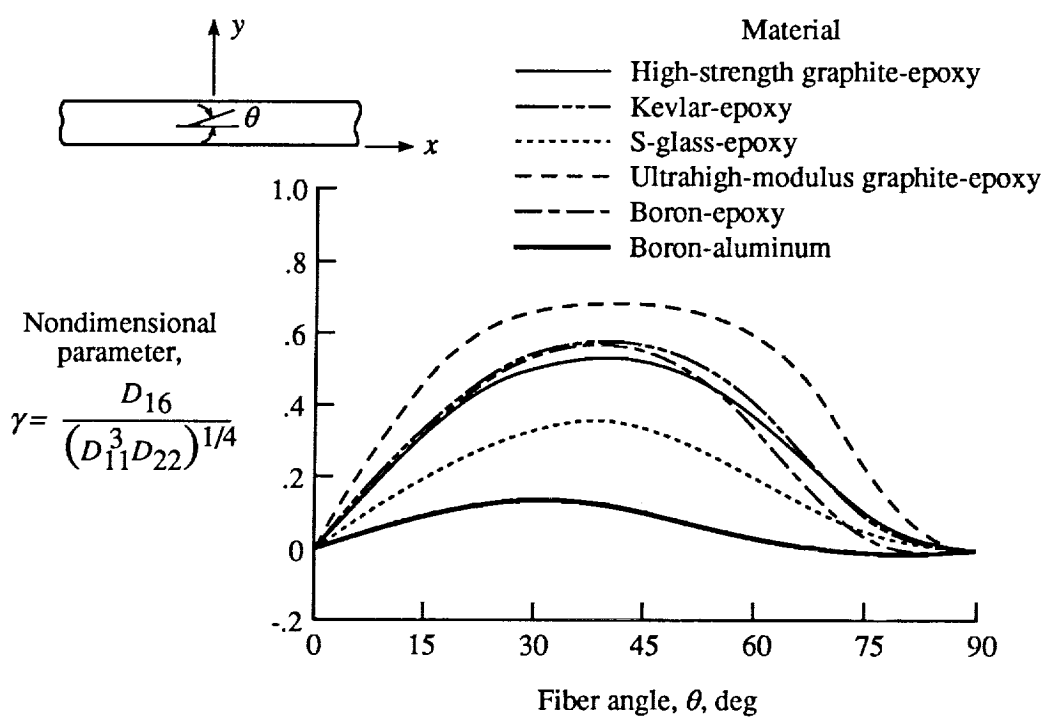

Figure 8. Effect of lamina material properties on nondimensional anisotropic parameter γ for $[\pm\theta]_s$ laminates.

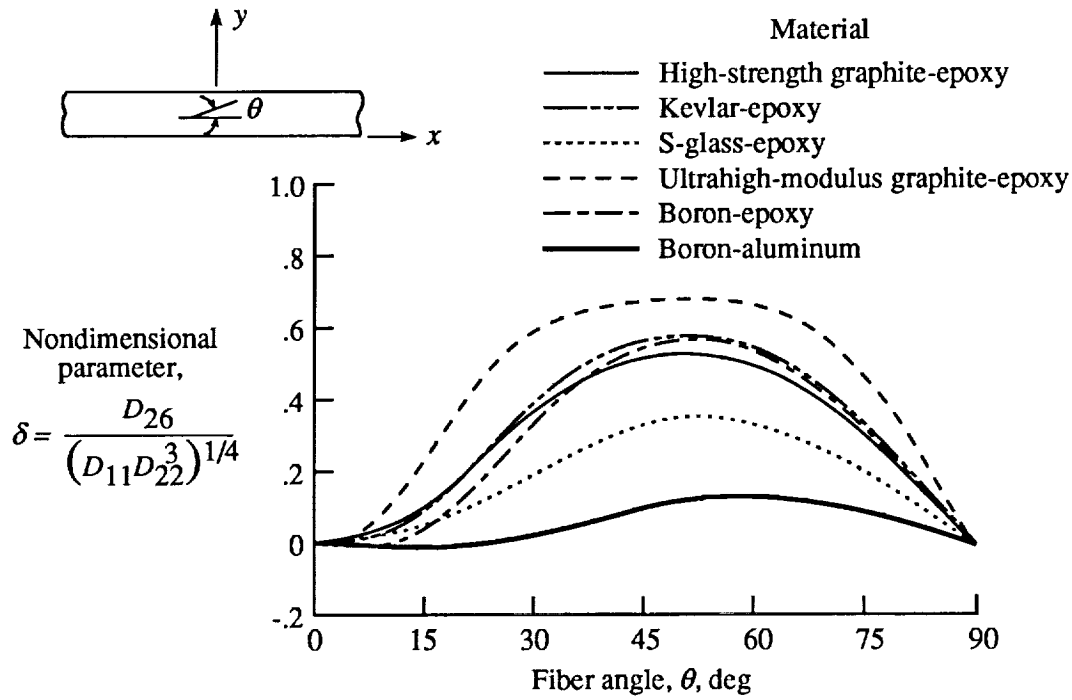

Figure 9. Effect of lamina material properties on nondimensional anisotropic parameter δ for $[\pm\theta]_s$ laminates.

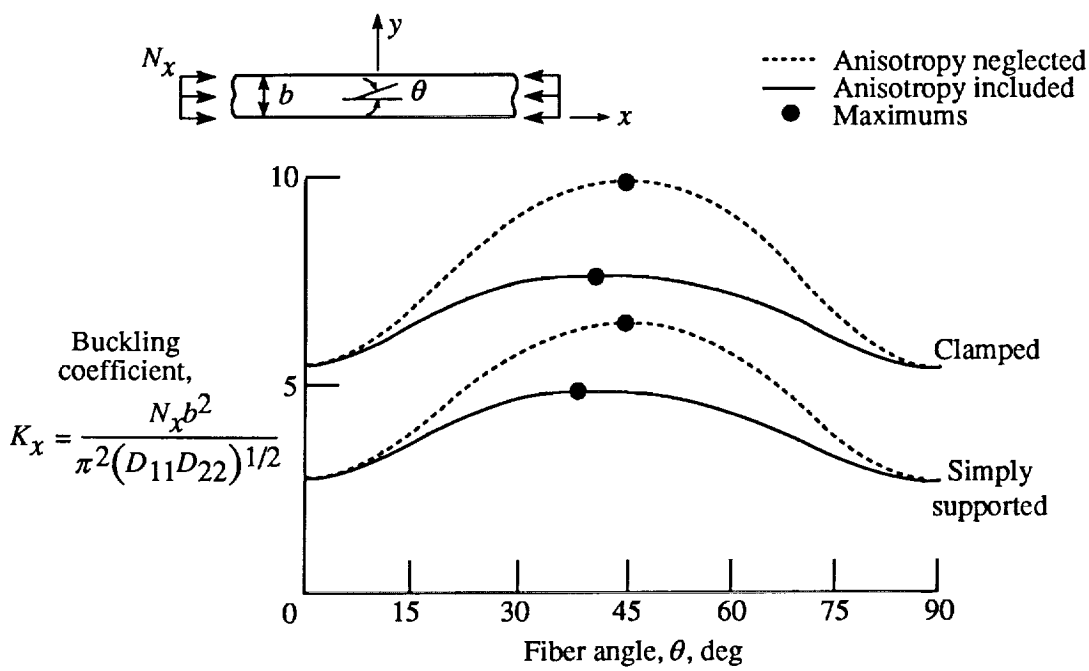

Figure 10. Buckling coefficients for axial-compression-loaded $[\pm\theta]_s$ graphite-epoxy laminates.

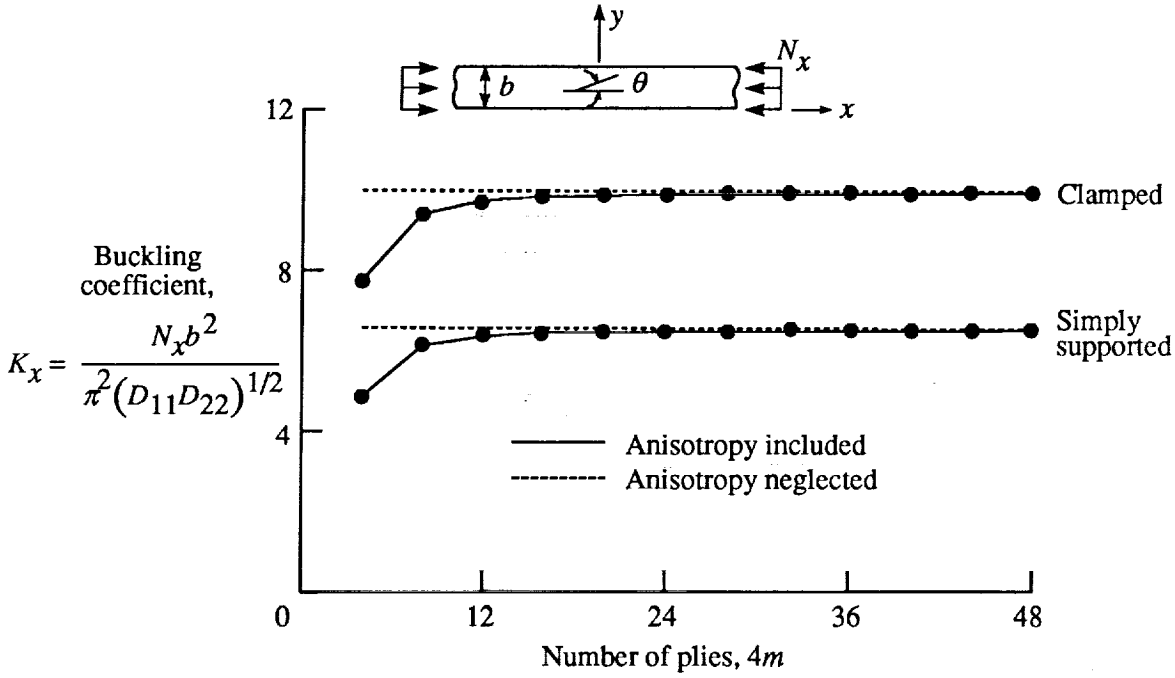

Figure 11. Buckling coefficients for axial-compression-loaded $[(\pm 45)_m]_s$ graphite-epoxy laminates.

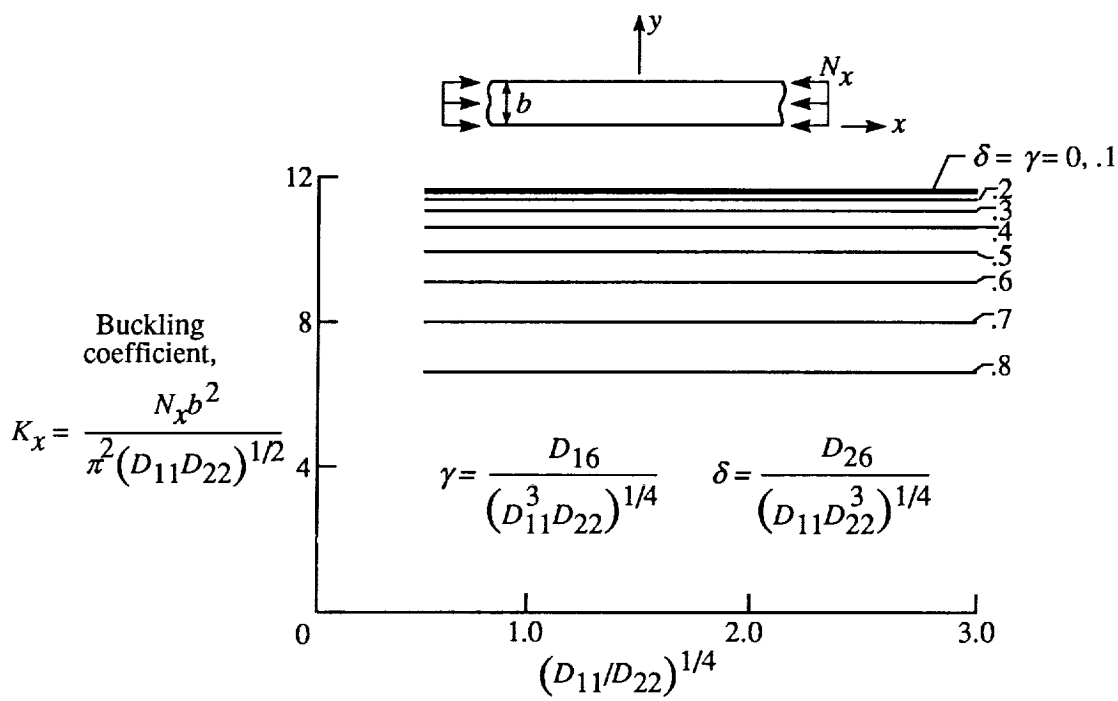

Figure 12. Effects of $(D_{11}/D_{22})^{1/4}$ and anisotropic parameters γ and δ on buckling coefficients for axial-compression-loaded clamped plates for $\beta = 3$.

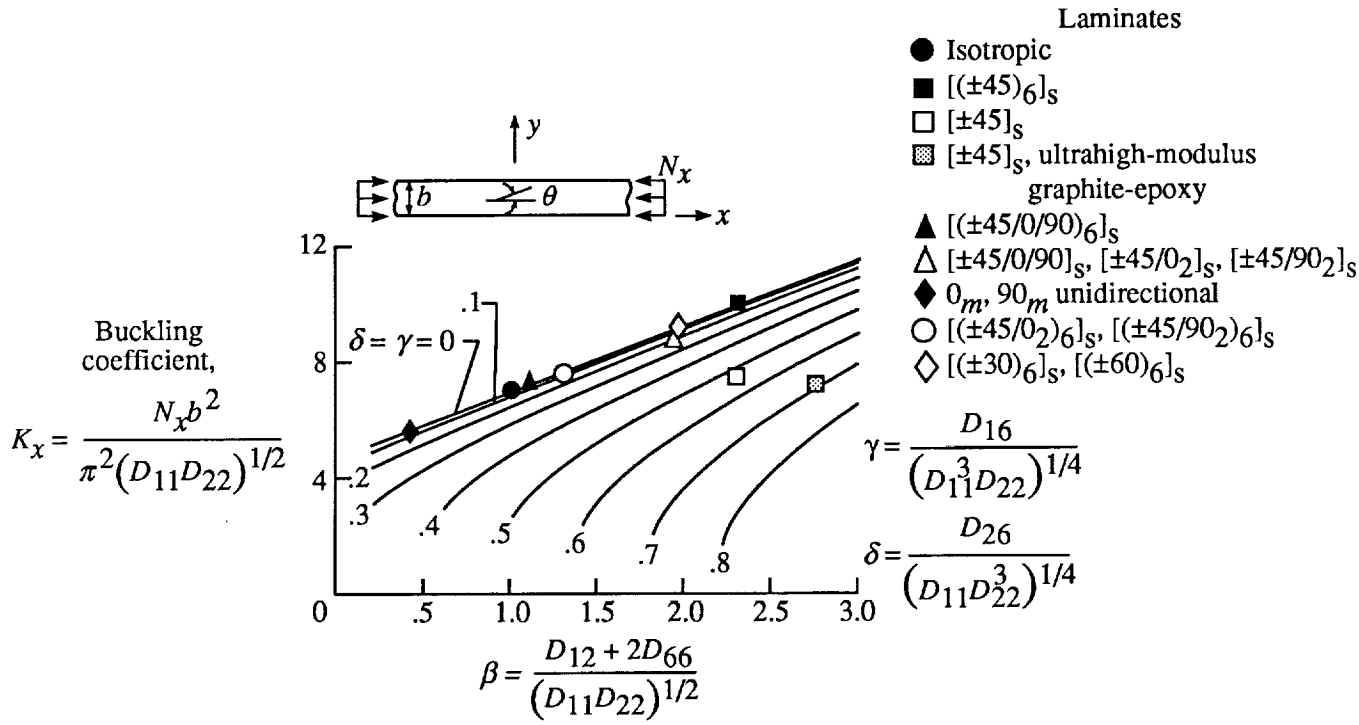

Figure 13. Effects of orthotropic parameter β and anisotropic parameters γ and δ on buckling coefficients for axial-compression-loaded clamped plates. All laminates shown are made of typical graphite-epoxy material unless otherwise noted.

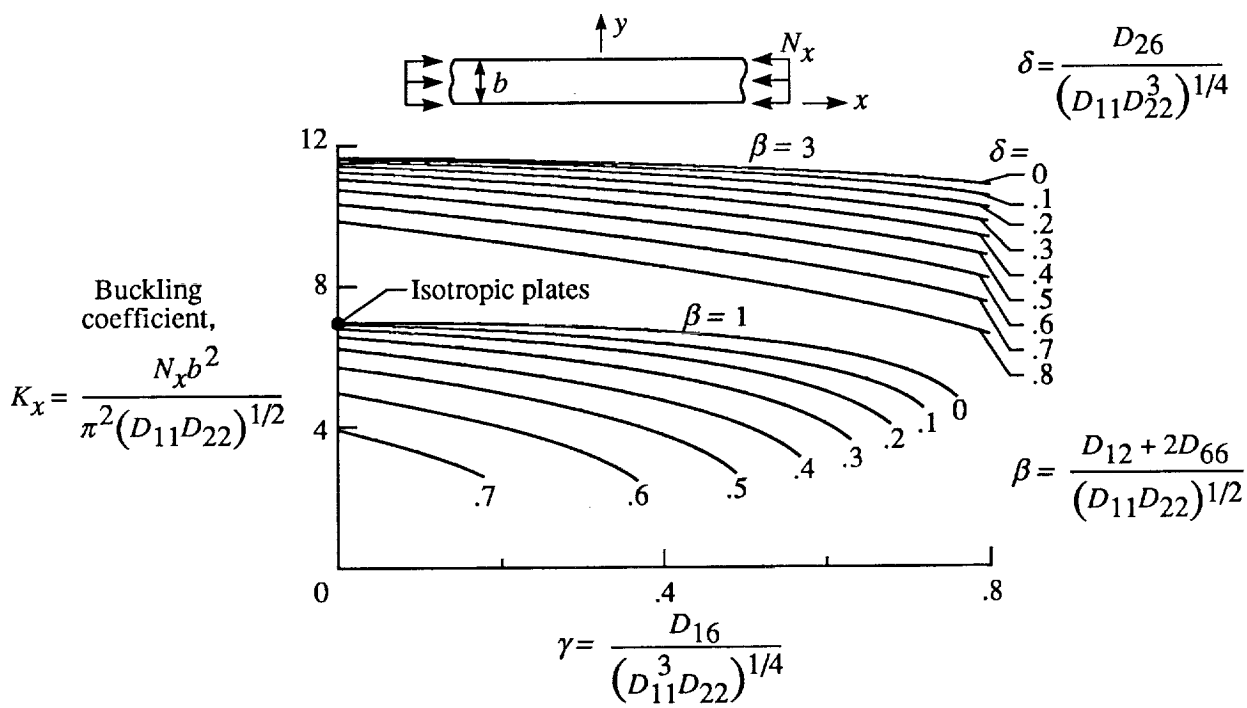

Figure 14. Effects of anisotropic parameters γ and δ on buckling coefficients for axial-compression-loaded clamped plates.

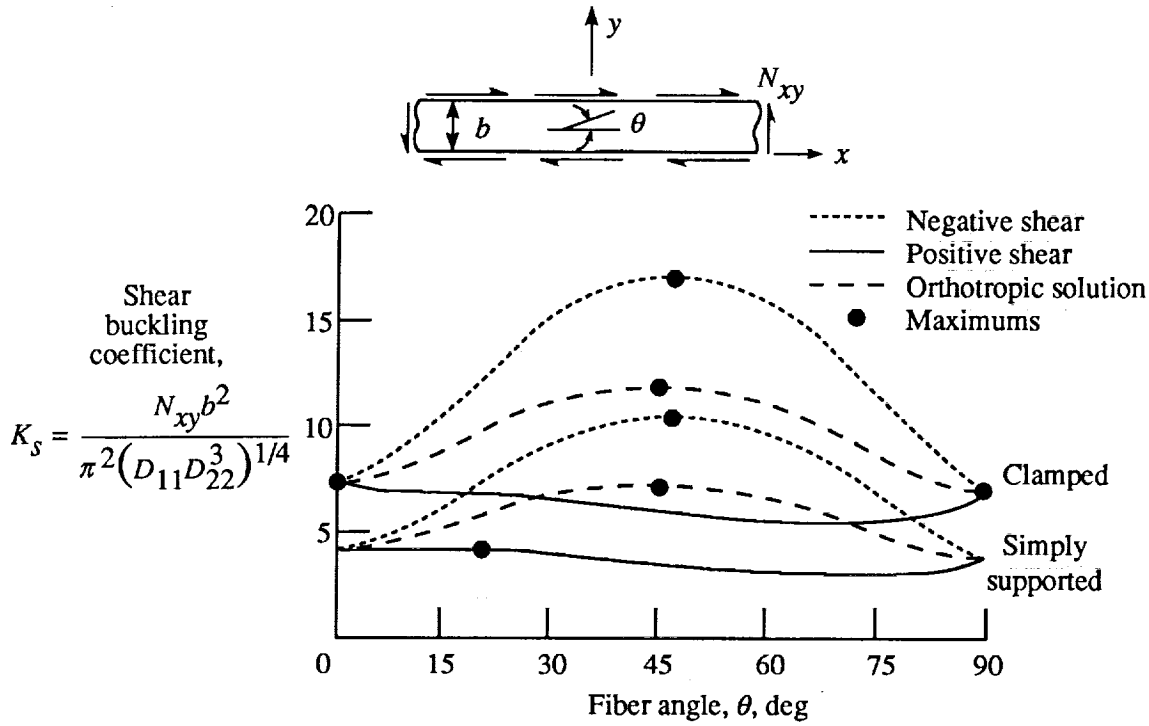

Figure 15. Buckling coefficients for shear-loaded $[\pm\theta]_s$ graphite-epoxy laminates.

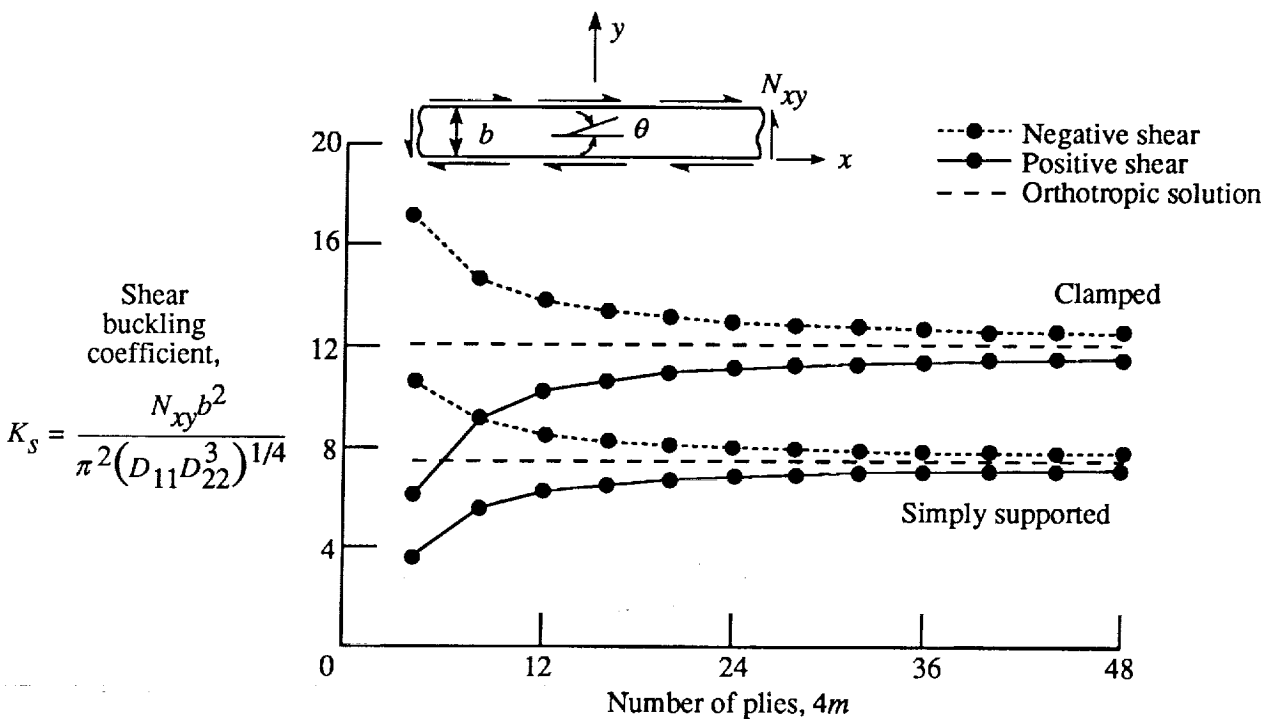

Figure 16. Buckling coefficients for shear-loaded $[(\pm 45)_m]_s$ graphite-epoxy laminates.

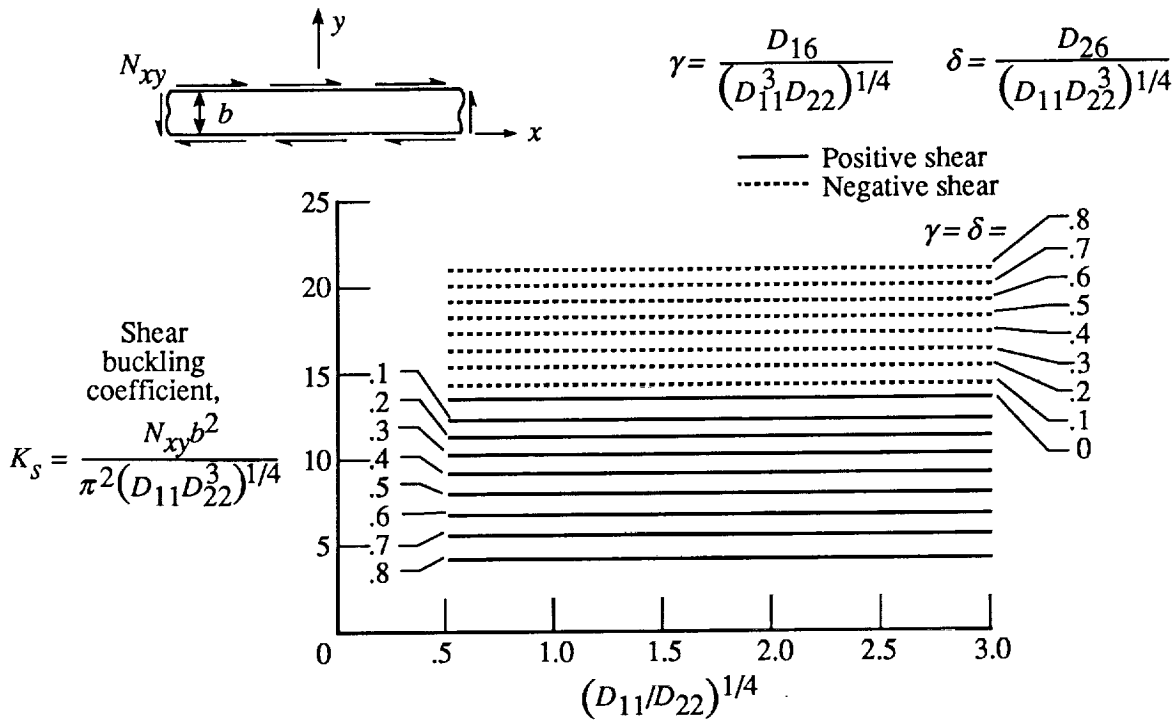

Figure 17. Effects of $(D_{11}/D_{22})^{1/4}$ and anisotropic parameters γ and δ on buckling coefficients for shear-loaded clamped plates for $\beta = 3$.

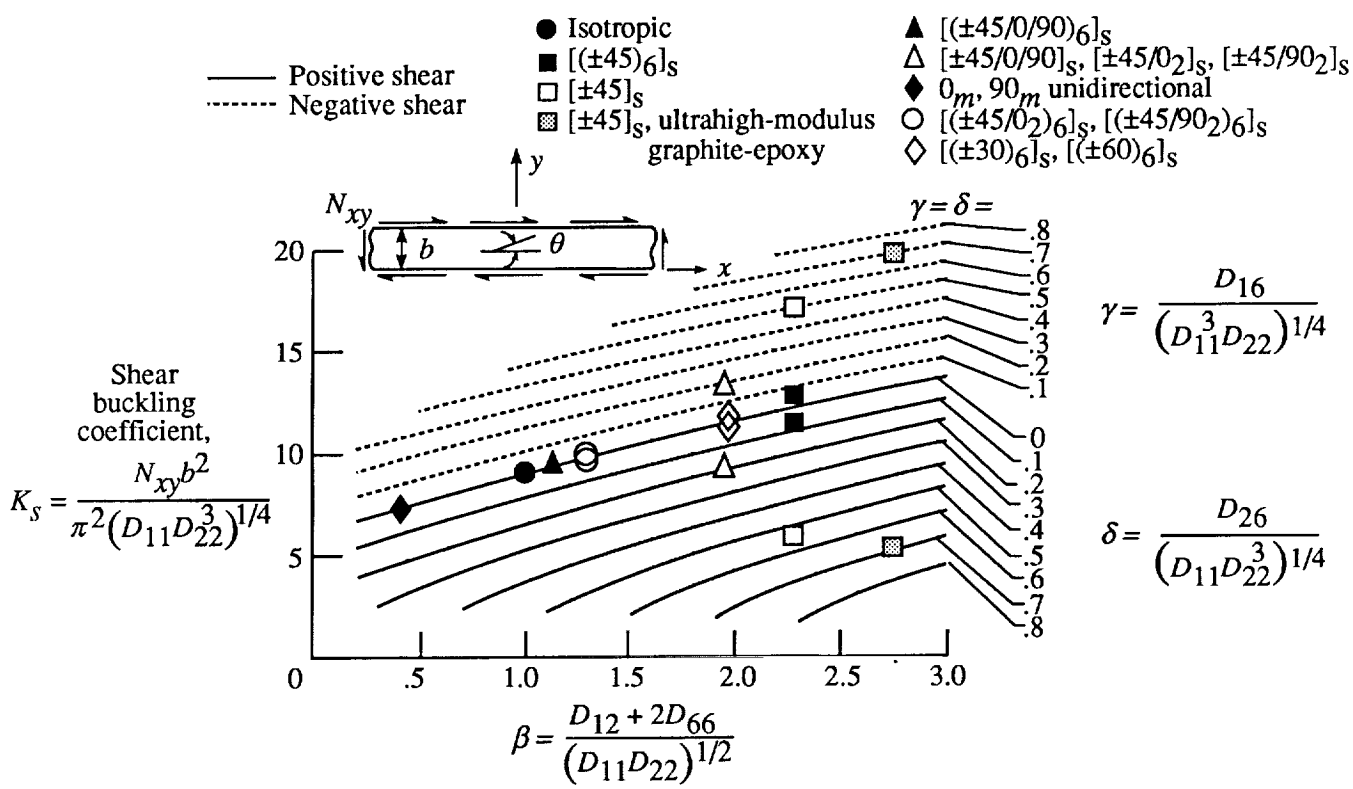

Figure 18. Effects of orthotropic parameter β and anisotropic parameters γ and δ on buckling coefficients for shear-loaded clamped plates. All laminates shown are made of typical graphite-epoxy material unless otherwise noted.

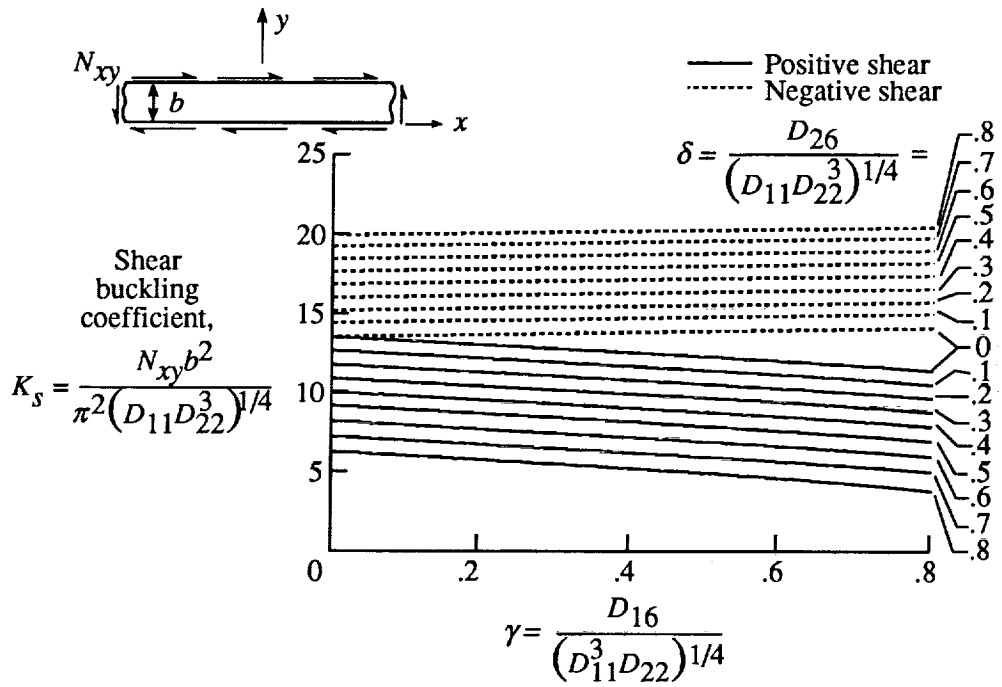

Figure 19. Effects of anisotropic parameters γ and δ on buckling coefficients for shear-loaded clamped plates for $\beta = 3$.

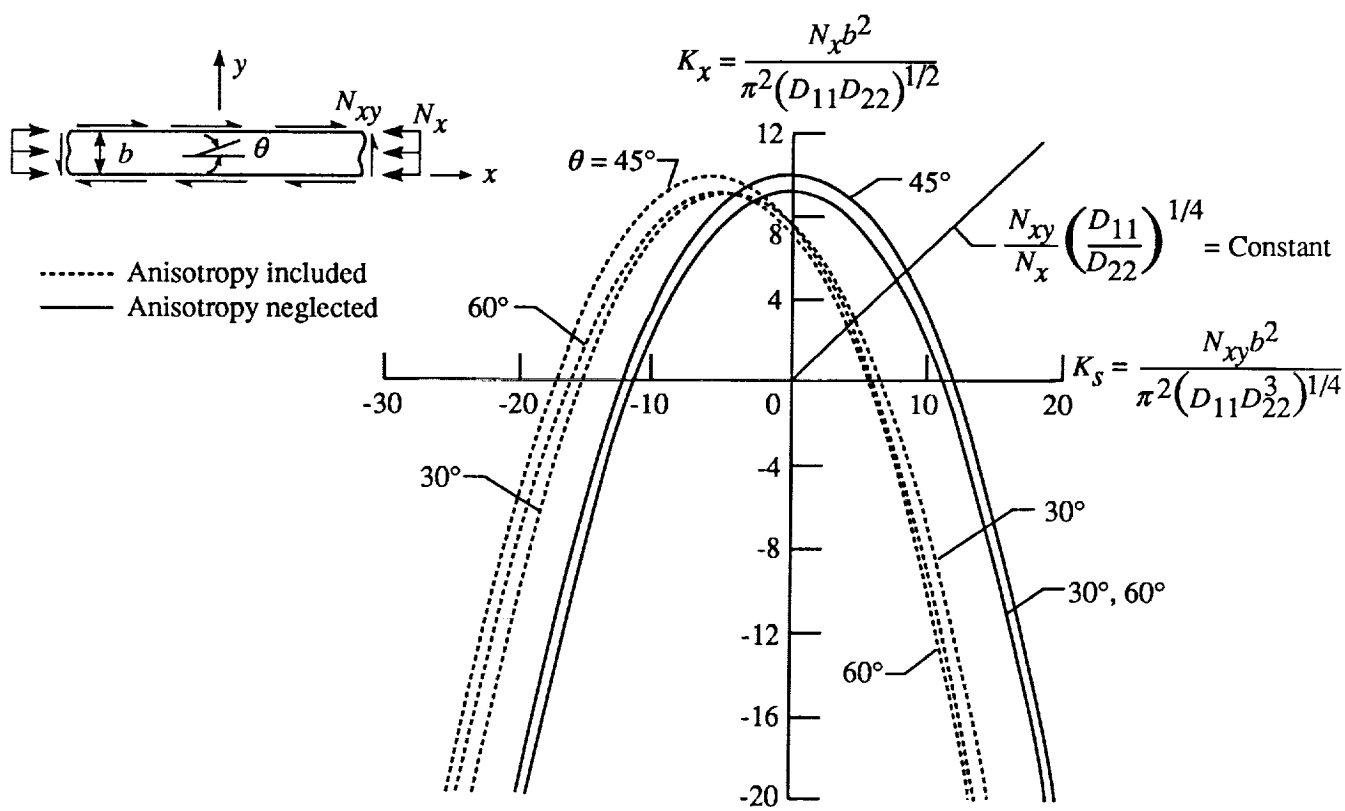

Figure 20. Buckling interaction curves for clamped $[\pm\theta]_s$ graphite-epoxy laminates subjected to axial tension or compression and shear.

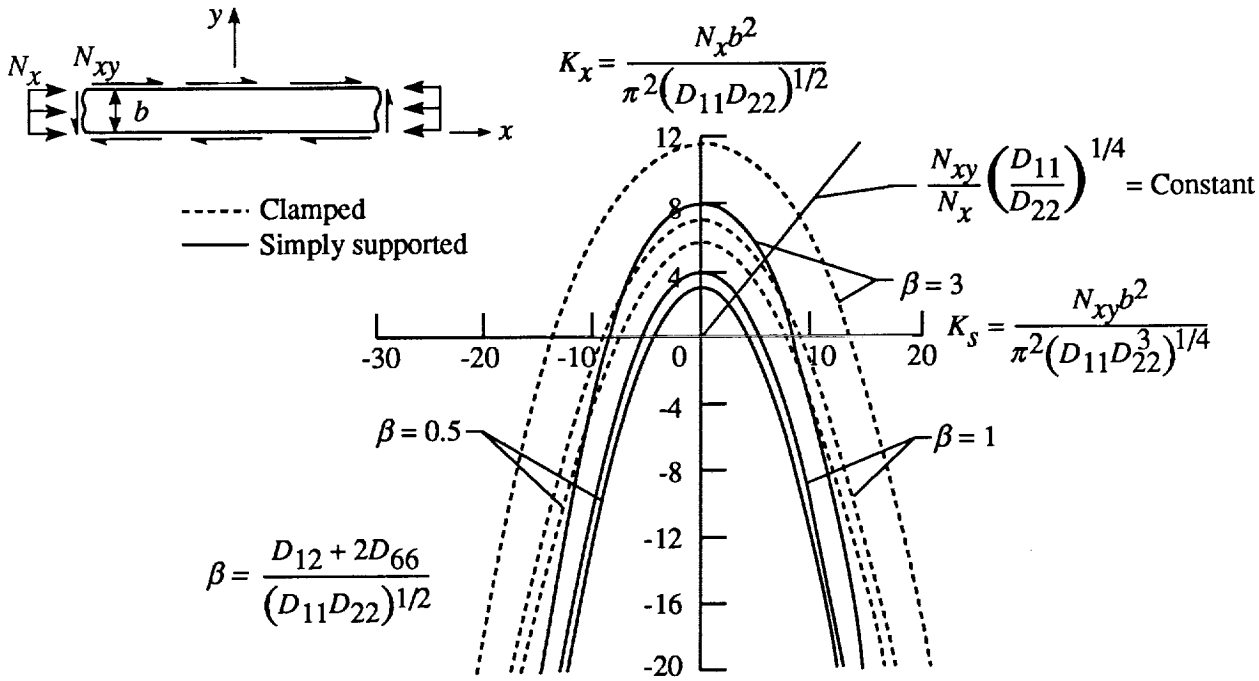

Figure 21. Effect of orthotropic parameter β on buckling interaction curves for specially orthotropic laminates ($\gamma = \delta = 0$) subjected to axial tension or compression and shear.

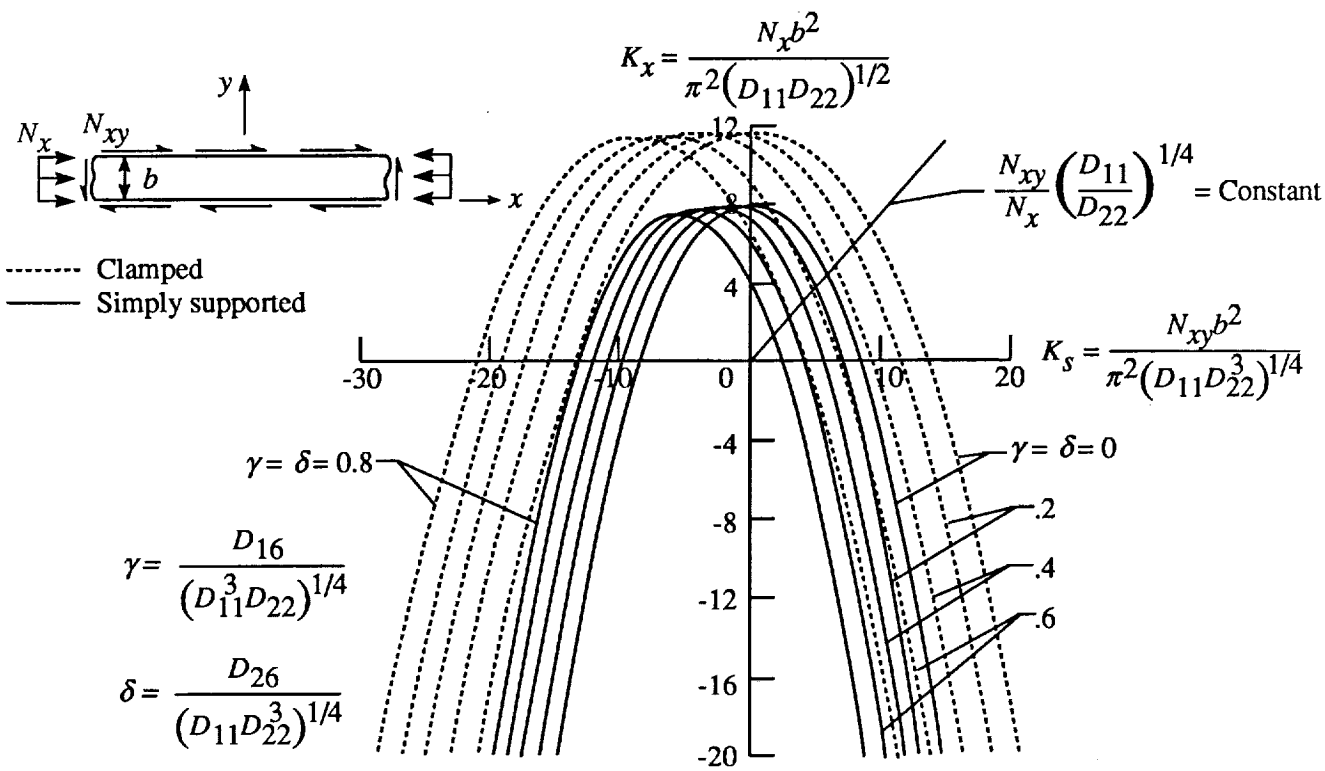

Figure 22. Effect of anisotropic parameters γ and δ on buckling interaction curves for laminates subjected to axial tension or compression and shear for $\beta = 3$.

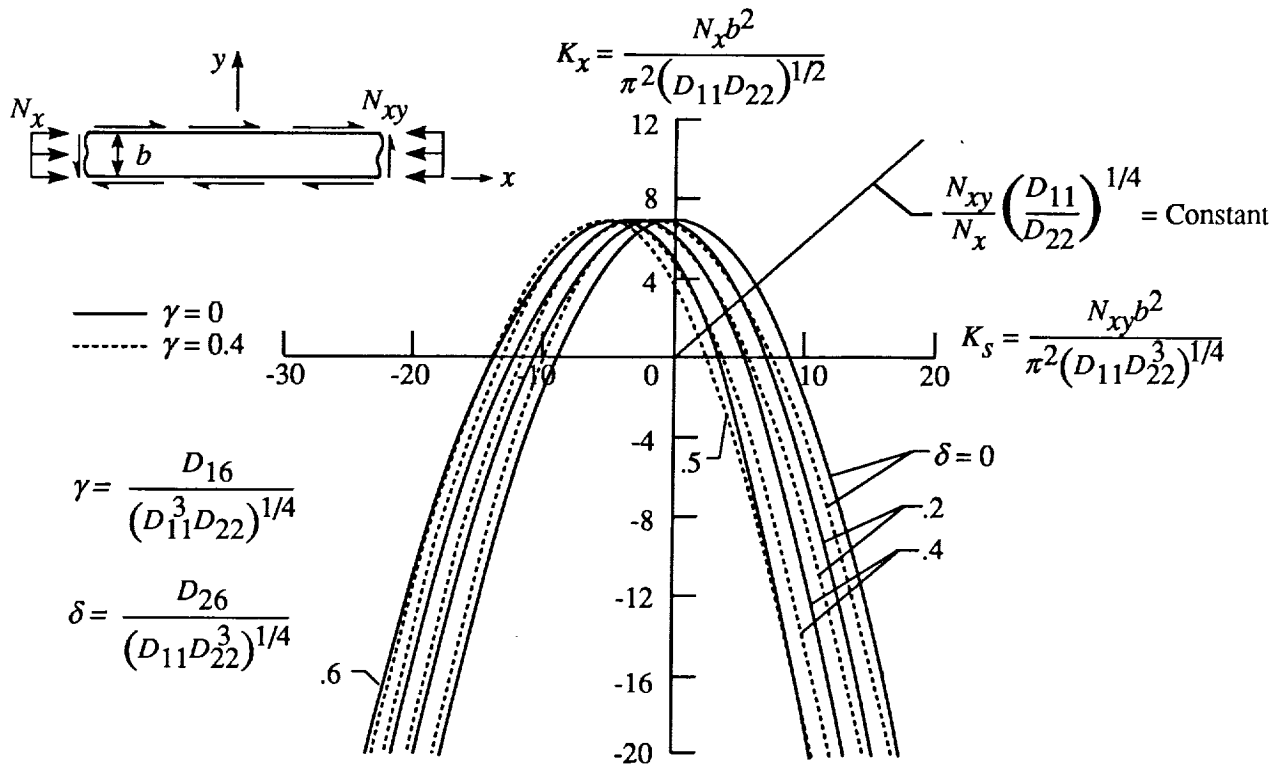

Figure 23. Effect of anisotropic parameters γ and δ on buckling interaction curves for clamped laminates subjected to axial tension or compression and shear for $\beta = 1$.

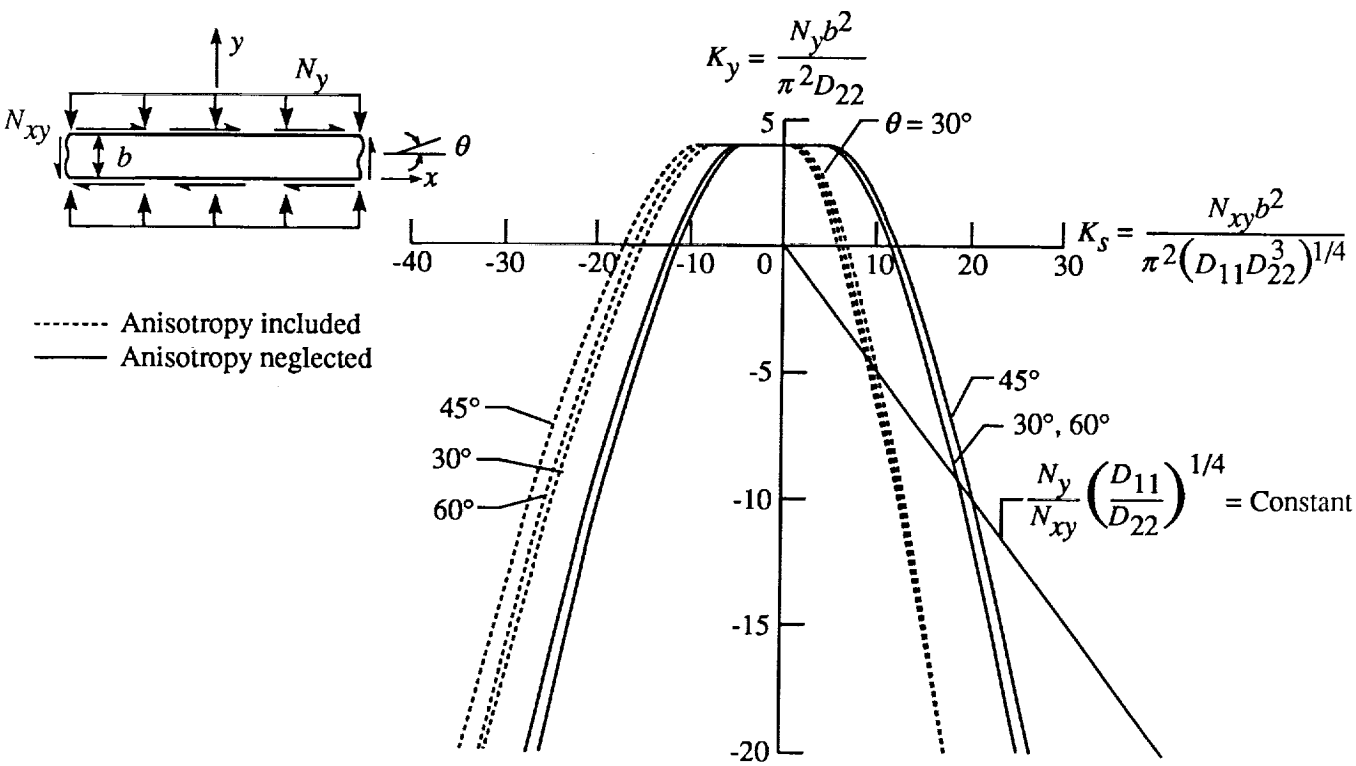

Figure 24. Buckling interaction curves for clamped $[\pm\theta]_s$ graphite-epoxy laminates subjected to transverse tension or compression and shear.

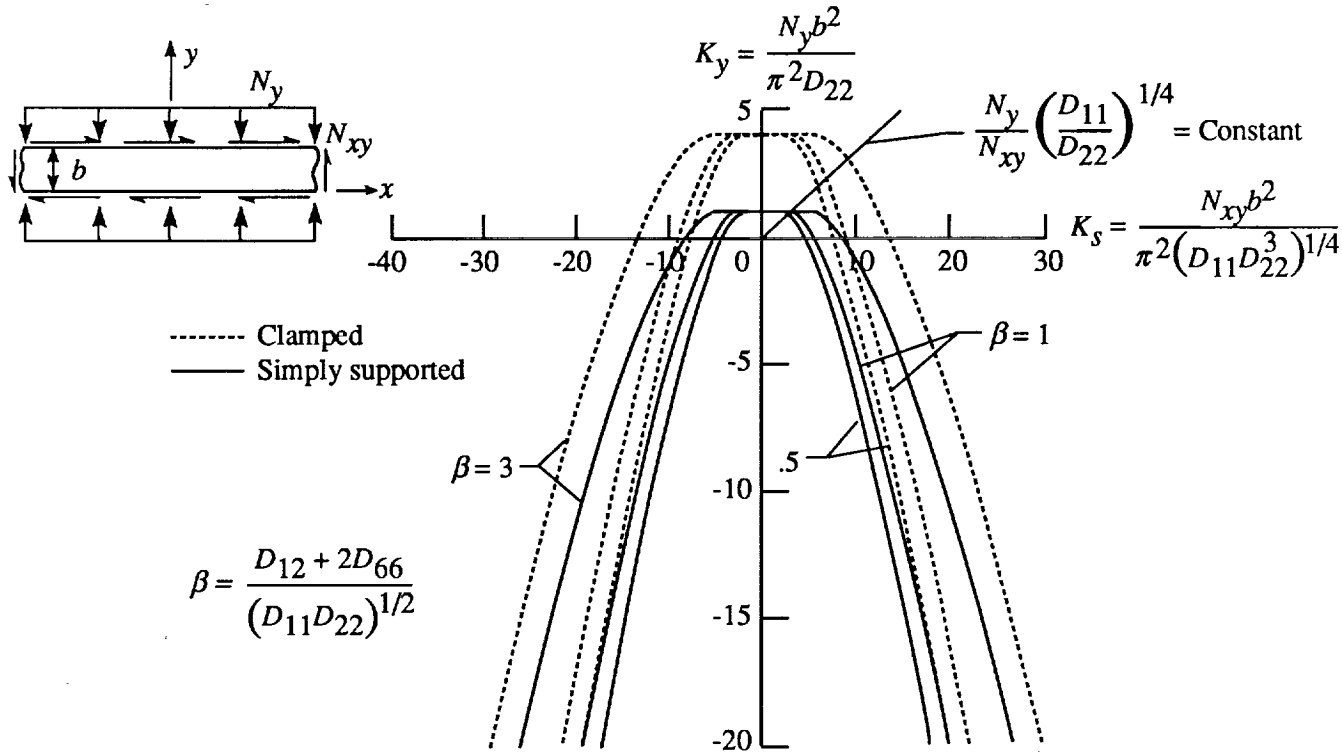

Figure 25. Effect of orthotropic parameter β on buckling interaction curves for specially orthotropic laminates ($\gamma = \delta = 0$) subjected to transverse tension or compression and shear.

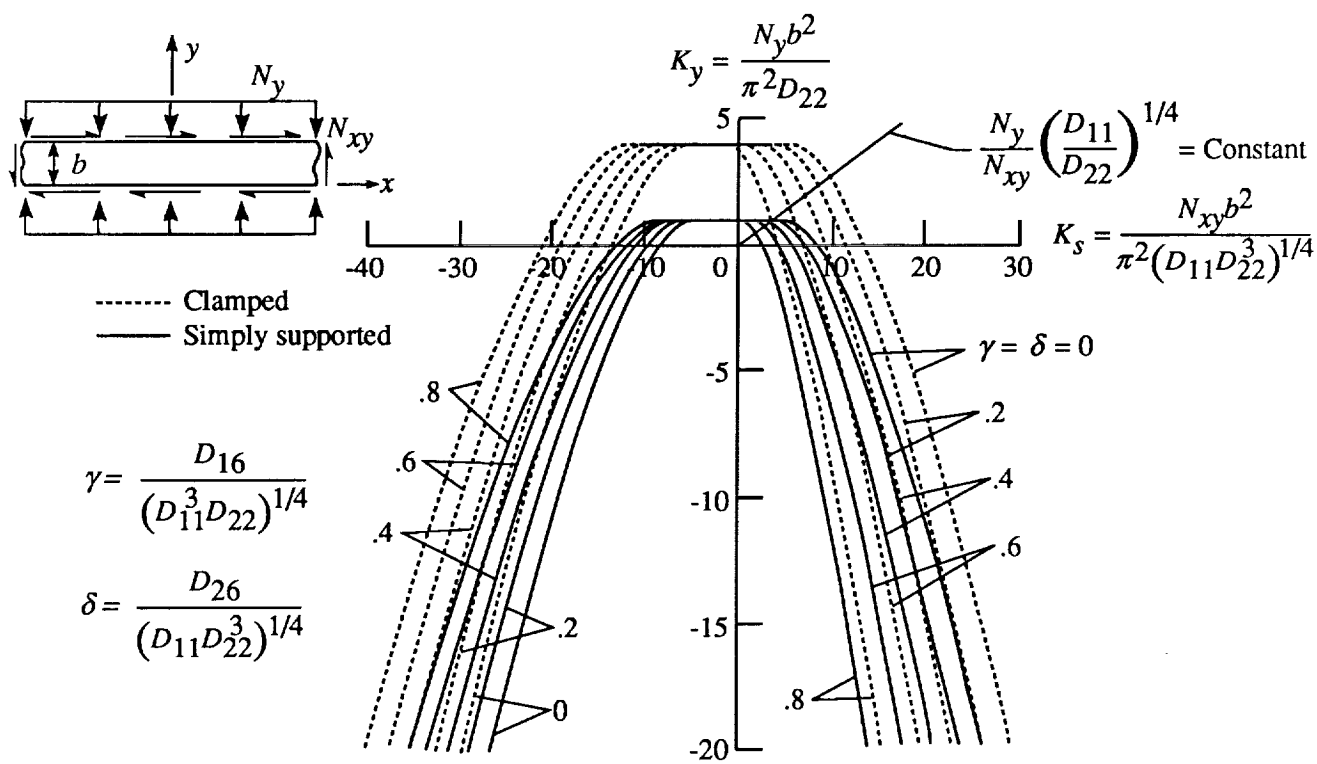

Figure 26. Effect of anisotropic parameters γ and δ on buckling interaction curves for laminates subjected to transverse tension or compression and shear for $\beta = 3$.

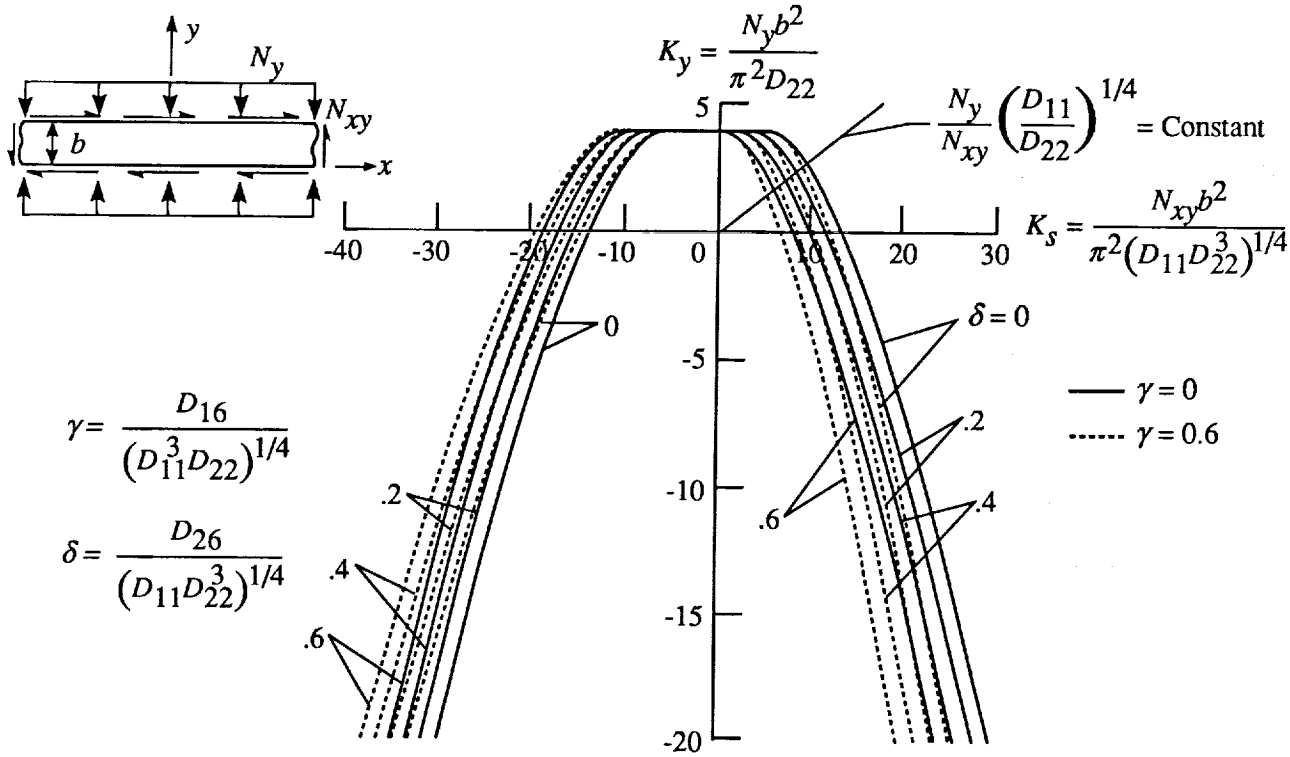

Figure 27. Effect of anisotropic parameters γ and δ on buckling interaction curves for clamped laminates subjected to transverse tension or compression and shear for $\beta = 3$.

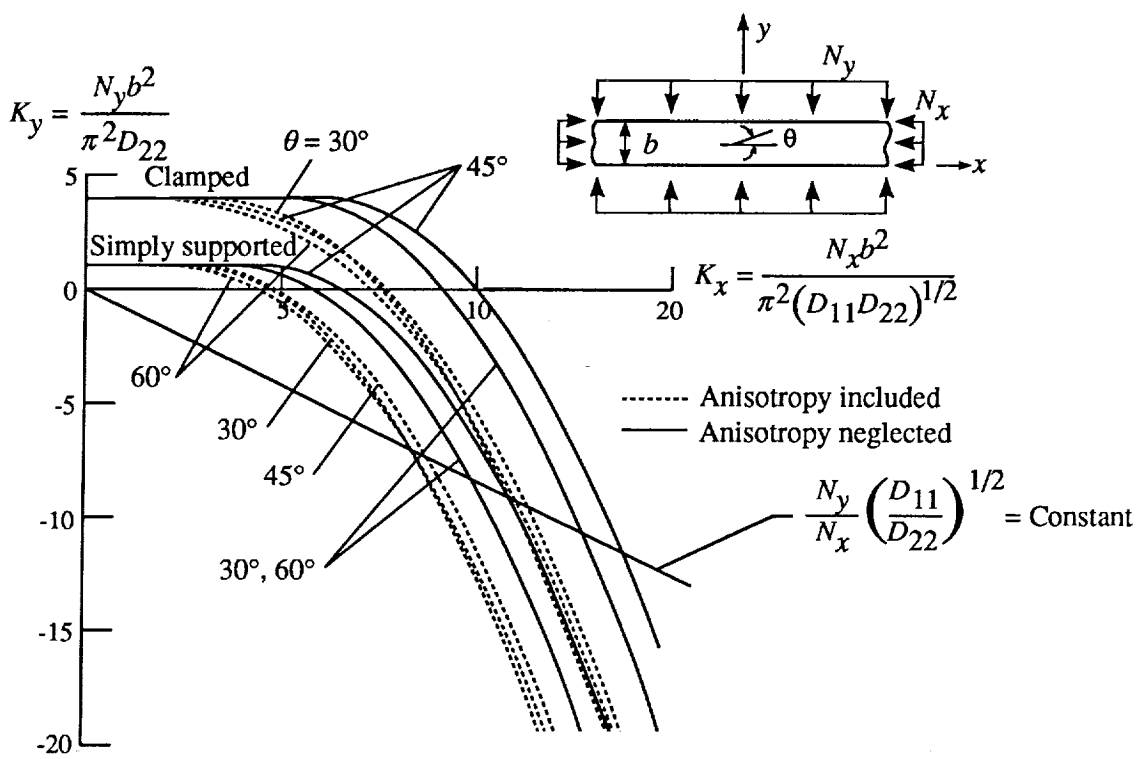

Figure 28. Buckling interaction curves for $[\pm\theta]_s$ graphite-epoxy laminates subjected to transverse tension or compression and axial compression.

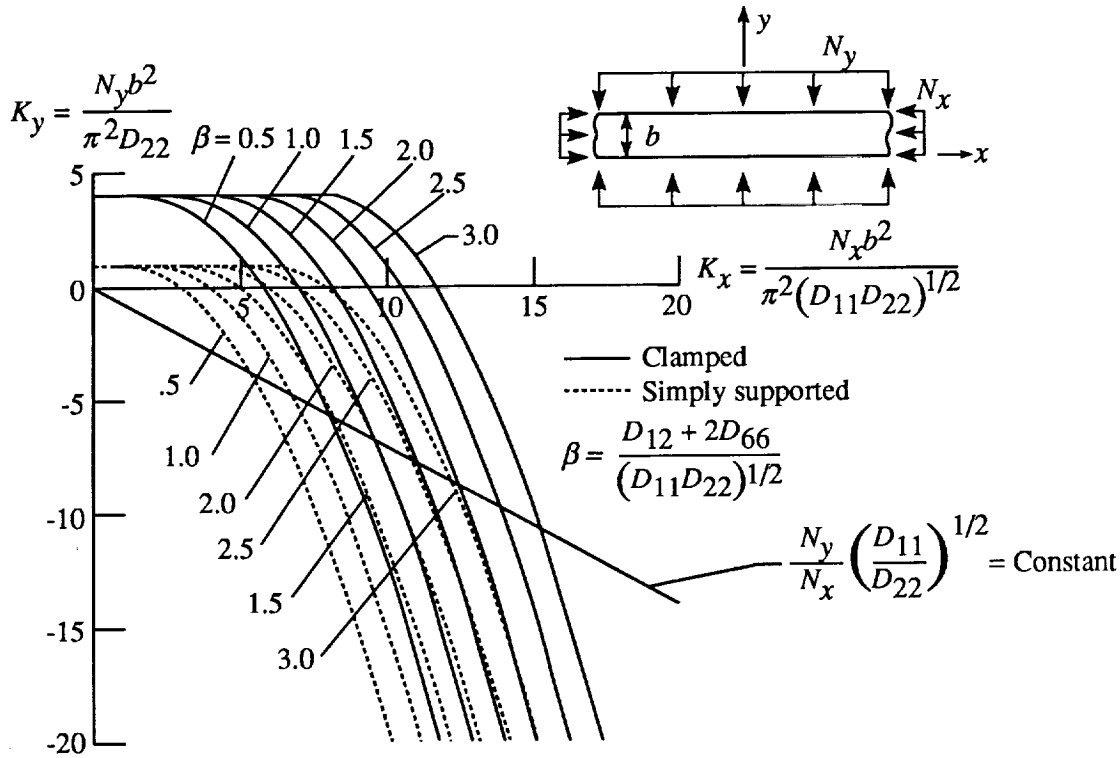

Figure 29. Effect of orthotropic parameter β on buckling interaction curves for specially orthotropic laminates ($\gamma = \delta = 0$) subjected to transverse tension or compression and axial compression.

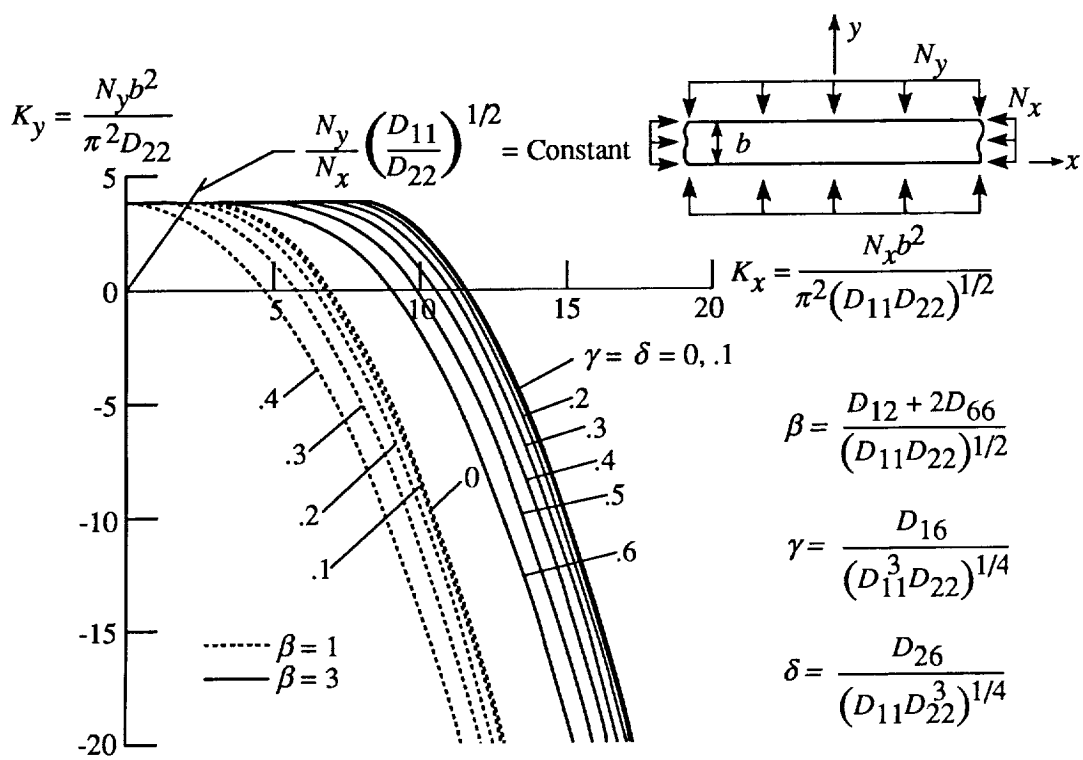

Figure 30. Effect of anisotropic parameters γ and δ on buckling interaction curves for clamped laminates subjected to transverse tension or compression and axial compression.

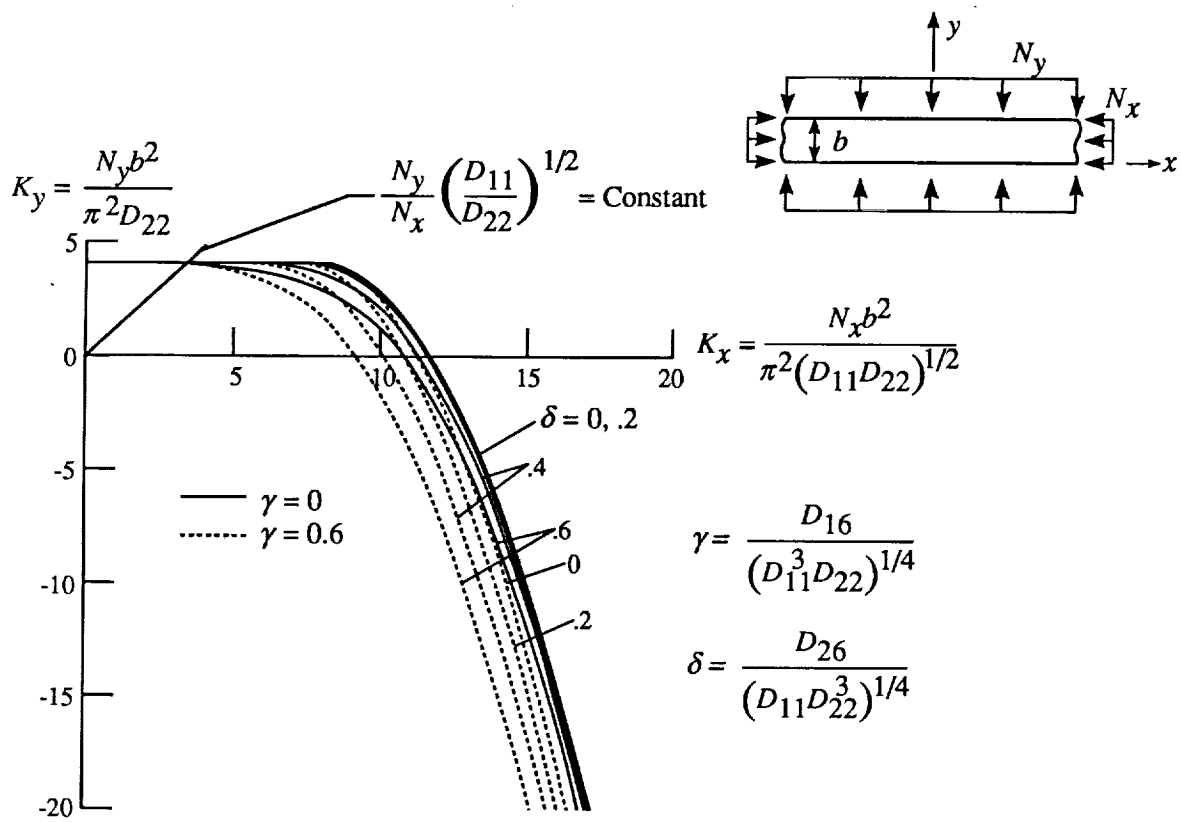

Figure 31. Effect of anisotropic parameters γ and δ on buckling interaction curves for clamped laminates subjected to transverse tension or compression and axial compression for $\beta = 3$.

REPORT DOCUMENTATION PAGE

Form Approved
OMB No. 0704-0188

Public reporting burden for this collection of information is estimated to average 1 hour per response, including the time for reviewing instructions, searching existing data sources, gathering and maintaining the data needed, and completing and reviewing the collection of information. Send comments regarding this burden estimate or any other aspect of this collection of information, including suggestions for reducing this burden, to Washington Headquarters Services, Directorate for Information Operations and Reports, 1215 Jefferson Davis Highway, Suite 1204, Arlington, VA 22202-4302, and to the Office of Management and Budget, Paperwork Reduction Project (0704-0188), Washington, DC 20503.

1. AGENCY USE ONLY *(Leave blank)*

2. REPORT DATE
May 1992

3. REPORT TYPE AND DATES COVERED
Technical Paper

4. TITLE AND SUBTITLE
Buckling Behavior of Long Symmetrically Laminated Plates Subjected to Combined Loadings

5. FUNDING NUMBERS
WU 505-63-50-07

6. AUTHOR(S)
Michael P. Nemeth

7. PERFORMING ORGANIZATION NAME(S) AND ADDRESS(ES)
NASA Langley Research Center
Hampton, VA 23665-5225

8. PERFORMING ORGANIZATION REPORT NUMBER
L-17035

9. SPONSORING/MONITORING AGENCY NAME(S) AND ADDRESS(ES)
National Aeronautics and Space Administration
Washington, DC 20546-0001

10. SPONSORING/MONITORING AGENCY REPORT NUMBER
NASA TP-3195

11. SUPPLEMENTARY NOTES
Presented at the Ninth DoD/NASA/FAA Conference on Fibrous Composites in Structural Design, Lake Tahoe, NV, Nov. 4–7, 1991.

12a. DISTRIBUTION/AVAILABILITY STATEMENT
Unclassified –Unlimited

Subject Category 24

12b. DISTRIBUTION CODE

13. ABSTRACT *(Maximum 200 words)*

A parametric study is presented of the buckling behavior of infinitely long, symmetrically laminated anisotropic plates subjected to combined loadings. The loading conditions considered are axial tension and compression, transverse tension and compression, and shear. Results obtained using a special-purpose analysis, well-suited for parametric studies, are presented for clamped and simply supported plates. Moreover, results are presented for some common laminate constructions, and generic buckling design charts are presented for a wide range of parameters. The generic design charts are presented in terms of useful nondimensional parameters, and the dependence of the nondimensional parameters on laminate fiber orientation, stacking sequence, and material properties is discussed. An important finding of the study is that the effects of anisotropy are much more pronounced in shear-loaded plates than in compression-loaded plates. In addition, the effects of anisotropy on plates subjected to combined loadings are generally manifested as a phase shift of self-similar buckling interaction curves. A practical application of this phase shift is that the buckling resistance of long plates can be improved by applying a shear loading with a specific orientation. In all cases considered in the study, the buckling coefficients of infinitely long plates are found to be independent of the bending stiffness ratio $\cancel{(D_{11}/D_{22})^{1/4}}$. (D sub 11/D sub 22) (1/4).

14. SUBJECT TERMS
Buckling; Combined loads; Anisotropy

15. NUMBER OF PAGES
29

16. PRICE CODE
A03

17. SECURITY CLASSIFICATION OF REPORT
Unclassified

18. SECURITY CLASSIFICATION OF THIS PAGE
Unclassified

19. SECURITY CLASSIFICATION OF ABSTRACT

20. LIMITATION OF ABSTRACT